NAL TR-1128T

ISSN 0389-4010
UDC 629.78
629.7.05
533.6.013

TECHNICAL REPORT OF NATIONAL AEROSPACE LABORATORY

TR-1128T

On Stability and Control of SSTO Spaceplane in Super- and Hypersonic Ascending Phase

Andreas DIEKMANN and Koichi MATSUSHIMA

November 1991

NATIONAL AEROSPACE LABORATORY

CHŌFU, TOKYO, JAPAN

On Stability and Control of SSTO Spaceplane in Super- and Hypersonic Ascending Phase*

by

Andreas DIEKMANN*1 and Koichi MATSUSHIMA*2

ABSTRACT

The natural dynamic stability of a single stage to orbit (SSTO) National Aerospace Laboratory Spaceplane Configuration is evaluated at seven refence points on a super-to hypersonic and constant dynamic pressure ascent trajectory. It is shown that dynamic instability occurs in the longitudinal and lateral motion during wide parts of the regarded trajectory. To counteract these instabilities a simple output feedback control is introduced to achieve a pole assignment of the dominant modes according to handling quality criteria commonly used for conventional aircraft. The sensitivity of augmented stability parameters to deviations in the feedback gain constants is evaluted.

The dynamic behaviour of stability augmented Spaceplane is investigated by numerical simulation of its longitudinal motion during an ascent in standard clear air turbulence. Results indicate the sufficient performance of the control design. The controlled elevator deflection angles remain small despite the severe natural instability which occurred during wide parts of ascent trajectory.

Keywords : Spaceplane, flight control, stability

概　要

単段式スペースプレーンとして、滑走路を用いて水平離陸したのち、エアブリージング・エンジンによって大気中でマッハ12あるいはそれ以上の高速まで加速され、大気層を出たあとはロケットエンジンによって所定の軌道に投入されるような宇宙輸送系を想定する。このようなスペースプレーンを具体的に実現させるためには、推進系をはじめとして構造・材料などの分野での大きな技術革新に期待するところ大であるが、一方離陸してからごく短時間のうちに、大気中でマッハ10を越える極超音速まで加速される飛行を考えると、安定性や操縦性など、飛行制御の面からも大きな技術課題を抱えることになると思われる。本報は実際の風洞データをもとに、スペースプレーンの超音速および極超音速領域の飛行における、安定性の予備的解析を行ったものである。

* received 26 July 1991

*1 Visiting researcher (European Communities Scientific Training Programme in Japan)

*2 Control Systems Division

解析に用いたデータは、航空宇宙技術研究所におけるスペースプレーン研究の一環として、ＮＡＬゼロ次モデルを用いて、平成元年度までに行われた風洞試験の結果である。

スペースプレーンの上昇軌道として、離陸したマッハ1.3程度で制限動圧に達した後は、動圧一定で上昇加速するものを仮定し、その動圧一定での飛行時における、マッハ1.5からマッハ12までの間の７つの基準点を選び、機体の動安定に関する解析を行った。その結果縦及び横の運動のいずれにも、不安定性が生じることを見出した。またこれを補償するために、簡単なフィードバック制御系を設計し、その結果を調べるために、スペースプレーンの飛行運動の数値シミュレーションを行い、満足すべき結果を得た。

1. INTRODUCTION

The concept of national Aerospace Laboratory Spaceplane (NALSP) aimes for a fully reusable single-stage-to orbit (SSTO) space transportation system with a horizontal launch mode. During atmospheric ascent, powered with airbreathing engines, the Spaceplane is scheduled to cross the Mach number range up to Mach 12. Due to its far aft center of gravity location, NALSP is expected to experience severe flight mechanical problems in the high Mach number and low angle of attack range because of longitudinal and lateral static instability in this flight range. In this paper the super- and hypersonic ascent (Mach 1.33-12) along a constant dynamic pressure trajectory, which is proposed in the literature (ref. 1) and is derived again in this paper, serves as reference condition for the analysis of NALSP's dynamic stability in super- and hypersonic flight.

After an evaluation of the dynamic characteristics of the unaugmented rigid Spaceplane a linear output feedback control law for the longitudinal and lateral motion is introduced. In a first step, the feedback design achieves a pole assignment to fixed locations inside a region of the complex plane marked 'desired' according to commonly used handling quality criteria. In a second step the feedback design allows a pole location within a region marked only 'acceptable' but moreover aimes to minimize the sum of squares of the feedback gain constants to achieve minimum control surface deflections. For both feedback designs, the sensitivity of the pole locations to changes in the feedback gain constants is evaluated.

Finally the ascent of Spaceplane in the longitudinal plane is simulated considering vehicle dynamics and the influence of standard atmospheric turbulence.

2. DESCRIPTION OF NATIONAL AEROSPACE LABORATORY SPACEPLANE

The geometry of Spaceplane (fig. 1), considered in this paper, has a double vertical tail wiht 60° dihedral and a retractable canard (ref. 2). Important geometrical data and mass properties are:

total length	—	64m
center of gravity location assumed during considered ascent phase	—	68% length from nose
wing span b	—	29.8m
mean aerodynamic chord c	—	17.6m
wing reference area S	—	532.5m²
take-off wieght	—	350tons

moments of inertia at take-off (ref. 3):

I_x — $5.71 \cdot 10^6$ kg m²
I_y — $3.77 \cdot 10^7$ kg m²
I_z — $4.21 \cdot 10^7$ kg m²

3. REFERENCE ASCENT TRAJECTORY

3. 1 Description of considered ascent trajectory phase

According to ref. 1 and sketched in fig. 2, after take-off Spaceplane will climb with a constant flight path angle of 3° (phase 1) towards a constant dynamic pressure trajectory (phase 2.)

Seven points on this constant dynamic pressure trajectory will serve later as reference points for a small perturbation analysis of Spaceplane dynamic stability during super- and hypersonic ascent. Phase 2 covers the Mach number range from Mach 1.33 towards Mach 12.

The value of constant dynamic pressure assumed in this paper (85 kPa) results from

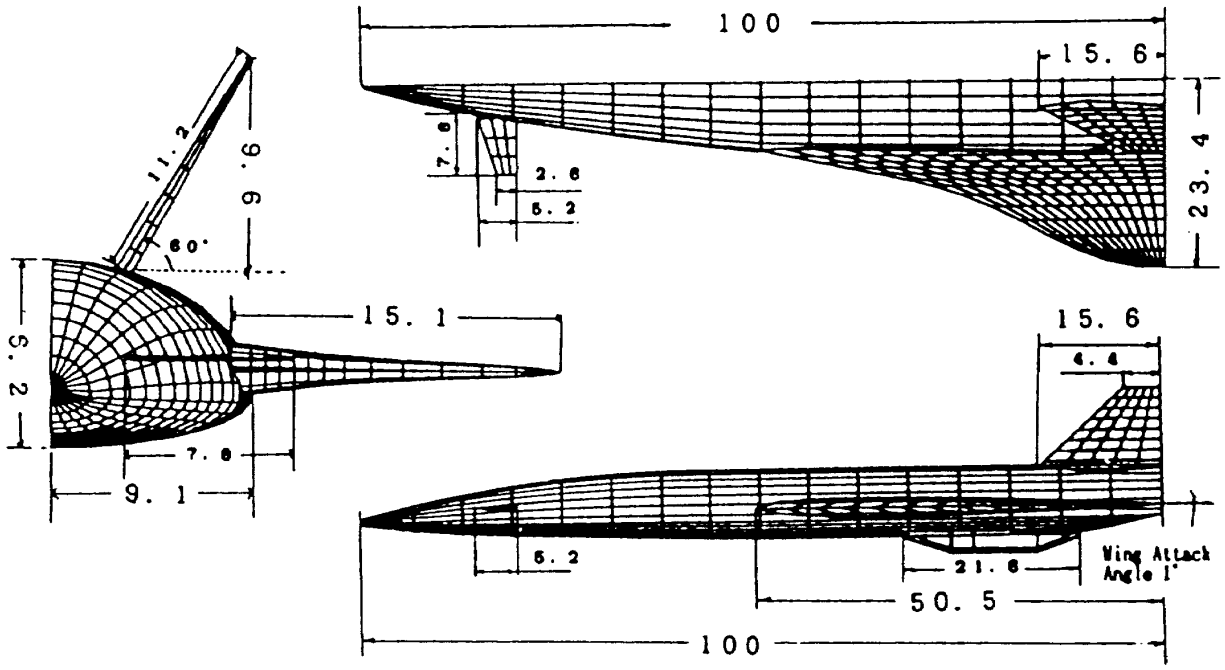

Fig. 1. Geometry of NAL Spaceplane (from ref. 2) (The model sizes are normalized by the body length and shown in %)

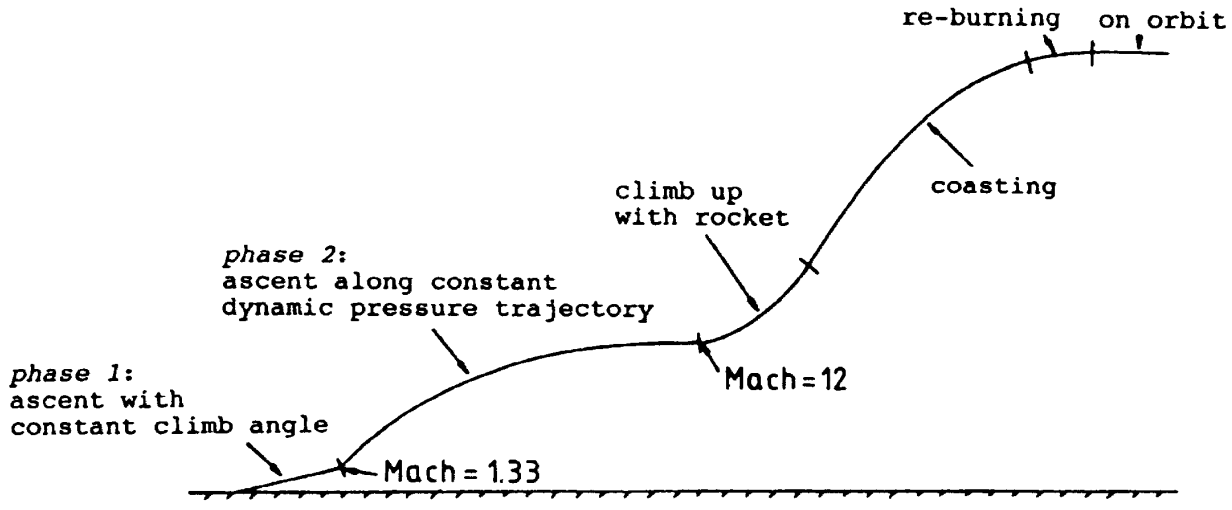

Fig. 2. Schematic diagram of Spaceplane ascent trajectory

scaling down the value proposed in ref. 1 (100kPa) according to the lower mass of Spaceplane assumed here (350 tons) conpared to 545 tons in ref. 1[1]. The downscaling of Q was done to maintain the dynamic similarity of both Spaceplane concepts. According to the underlying similarity law (see for ex.: GAINER, T.G,; SHERWOOD, H.; NASA SP-3070, 1972), if N is the scale factor for geometric length, then N^3 is the scale factor for the vehicle mass, $\sqrt{N}$ is the

1) The lower mass of Spaceplane was chosen in accordance with more recent Spaceplane concepts (ref.4)

one for the velocity and N the one for Q.

3. 2 Computation of reference ascent trajectory

Considering Spaceplane as a mass point, the reference trajectory is described by the velocity V, the flight path angle ν (see fig. 3) and the flight altitude h. Because of the requirement for constant dynamic pressure Q throughout the considered trajectory phase, it is convenient to use the dynamic pressure as a state variable instead of the altitude. For a given flight velocity, the dynamic pressure and the flight altitude are connected by the altitude dependent air density. By employing Q as a state variable and because of $\dot{Q} = 0$, the differential equation for the altitude h is equivalently replaced by an a algebraic expression.

The trajectory control variables are the angle of attack α and the thrust T. Assuming an ascent in a longitudinal plane and eastward along the equator, the equations of motion are:

$$\dot{V} = \frac{T}{m}\cos\alpha - g\sin\nu - \frac{Q}{m}SC_D \qquad (1)$$

$$\dot{\nu} = \frac{T}{mV}\sin\alpha - \frac{g}{V}\cos\nu + \frac{V}{R}\cos\nu + \frac{Q}{mV}SC_L \qquad (2)$$

$$\dot{Q} = -\frac{V}{h_s}Q\sin\nu + \rho\dot{V}V = 0 \qquad (3)$$

$$\dot{m} = -\frac{T}{I_{sp}\,g} \qquad (4)$$

Eqn. (4) describes the time dependency of Spaceplane's mass.

The drag and lift coefficients (C_D and C_L) are functions of the angle of attack (α) and Mach number (M). The thrust (T) and specific impuls (I_{SP}) are functions of the altitude (h) and Mach number.

The thrust vector is assumed to be aligned with the body-fixed x-axis (for the coordinate system see fig. 3). R is the radius of the earth.

Introducing the following models for the altitude dependent airdensity ρ (ref. 26) and atmospheric pressure p (ICAO Standard Atmosphere, NASA rep. 1235), (h in [km]):

$$\rho = \rho_0 \exp(-h/h_s) \qquad h_s = 7.092\ \text{km} \qquad (5)$$

$$p = p_0\,(1 - 0.0226\,h)^{5.255} \qquad h < 11\text{km} \qquad (6)$$

$$p = p_0\,1.26343\exp(-.1578\,h) \qquad h \geq 11\text{km}$$

(ρ_0 and P_0 are the atmospheric density and pressure on the ground, here assumed to be $\rho_0 = 1.225\text{kg}/\text{m}^3$, $p_0 = 10^5\ \text{N}/\text{m}^2$)
and regarding the following formulas for the Mach number M and the dynamic pressure Q:

$$M = V/\text{sqrt}(\tau p/\rho) \qquad (7)$$

$$Q = 1/2\,\rho V^2 \qquad (8)$$

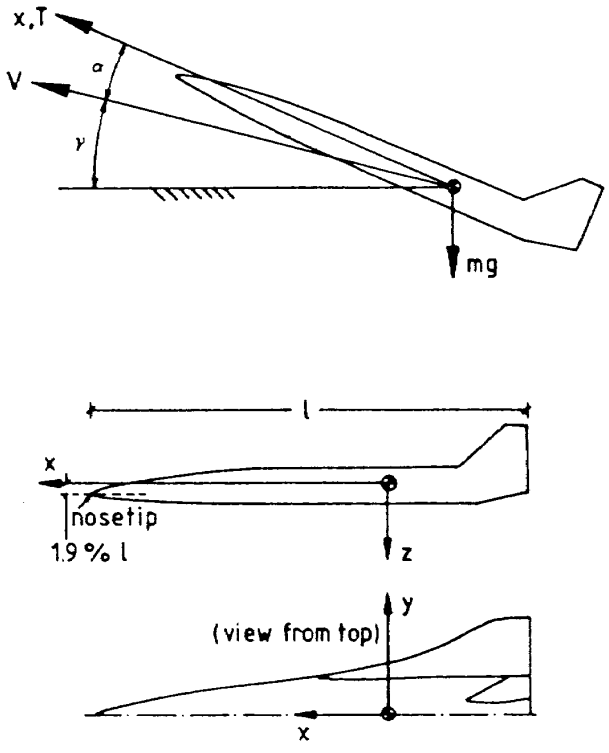

Fig. 3. Body-fixed coordinate system

where τ is the ratio of specific heats ($\tau = C_p/C_v$, for air: $\tau = 1.4$), from eqn. (7) and (8) the following formula for Q can be derived:

$$Q = 1/2\, M^2 \tau p \tag{9}$$

which, by use of eqn. (6), leads to two equations for the altitude h(in [km]):

$$h = 44.25 \left[1 - \left(\frac{2Q}{p_0 \tau M^2} \right)^{1/5.255} \right] \tag{10}$$

$$(h < 11\text{km})$$

$$h = -6.34 \ln \left(\frac{2Q}{1.26343\, M^2 \tau p_0} \right) \tag{11}$$

$$(h \geq 11\text{km})$$

Besides the requirements of:

$$Q = 85\,\text{kpa} \quad \text{and} \quad \dot{Q} = 0$$

valid for the entire super- and hypersonic ascent trajectory (phase 2 in fig. 2), the initial conditions (index 'I') of phase 2 are defined by the end conditions of phase 1:

$$M_I = 1.33$$

$$\nu_I = 3^\circ, \quad \dot{\nu}_I = 0$$

$$m_I = 332.5 \text{ ton}$$

The initial condition $\dot{\nu} = 0$ results from the requirement for a smooth transition between the constant flight path angle trajectory (phase 1) and constant dynamic pressure trajectory (phase 2).

From these given initial conditions and the initial values for the altitude and air density from eqn. (10) and (5), the initial values for the thrust and angle of attack can be computed from eqn. (1) and (2) by using eqn. (3) for the initial value of $\dot{V}$.

The initial thrust evaluated in this way is lower than the maximum thrust available at the initial altitude and Mach number according to the thrust model (ref. 5,6) used in this paper:

$$T_{max} = AB\, 9.63\ (N) \tag{12}$$

$$A = (-190\,h + 8000) / (0.012\,h^2 + 1)$$

$$B = -1.227\,M^3 + 25.77\,M^2 + 12.0$$

$$I_{sp} = CD/3000\ (s) \tag{13}$$

$$C = -0.035\,h^3 + 0.05\,h^2 + 53\,h + 2200$$

$$D = (666.7\,M + 2200) / (0.035\,M^2 + 1)$$

In this paper it is assumed that the thrust is increased linear in time within 60 seconds to its maximum value given in eqn. (12) and later always assumes its maximum possible value:

$$T = T_I + t/60\,s\ (T_{max} - T_I), \quad (0\,s \leq t \leq 60\,s) \tag{14}$$

$$T = T_{max}, \quad (t > 60\,s)$$

By that assumption, the number of trajectory control variables is reduced to one, i.e. the angle of attack.

Because of the requirement of $\dot{Q} = 0$ throughout the considered trajectory phase, eqn. (1) and (3) can be combined to form an implicit algebraic equation for the angle of attack necessary to achieve constant dynamic pressure for a given thrust:

$$\dot{Q} = 0 = -\frac{V}{h_s} Q \sin\nu + \frac{\rho V}{m} \left(T \cos\alpha - QSC_D - mg \sin\nu \right) \tag{15}$$

The set of equations to be solved for the computation of the reference trajectory finally are the differential eqn. (1), (2) and (4) with the initial conditions:

$V_I = 462.1$ m/s, $\nu_I = 3°$, $m_I = 332.5$ to

and the algebraic equations:

Eqn. (10) or (11) for h
Eqn. (5) for ρ
Eqn. (7) for M
Eqn. (15) for α

Eqn. (15) can be written as follows:

$$m\left(\frac{Q}{\rho h_s} + g\right)\sin\nu = T\cos\alpha - QSC_D \qquad (15')$$

Because of eqn. (14), in eqn. (15') the angle of attack α is the only independent variable. The left side in eqn. (15') and the drag-coefficient (C_D) are always positive, therefore, for certain combinations of thrust and flight path angle, there might be no solution for the angle of attack to fulfill eqn. (15'), i.e. to maintain constant dynamic pressure. The only way out in this case would be to increase the thrust. The employment of a thrust model as assumed in eqn. (12) and (14) is therefore only possible if the maximum thrust curve as a function of Mach number and altitude has a shape which always allows a solution for the angle of attack in eqn. (15'). The thrust model used in this paper shows to have this property.

The aerodynamic data (lift and drag) used during the trajectory computation are polynomial expansions with coefficients depending on the angle of attack and Mach number (tab. 1 from ref. 2). These coefficients are derived from windtunnel measurements carried out in the National Aerospace Laboratory at the Mach numbers 1.5, 2, 2.5, 3, 3.5, 4 and 7.1. The coefficients for the Mach numbers 10 and 12 are gained by extrapolation.

During trajectory computation the measured drag coefficients listed in tab.1 are increased by 10 precent to compensate for the neglecting of the engine intake area during the windtunnel tests.

3. 3 Reference ascent trajectory results

From eqn. (10) the initial altitude for phase 2 is computed to:

$h_I = 3057$ m [2)]

Table 1 Coefficients of polynomial expansions for C_D and C_L (ref.2)

$C_D = A_1 + A_2\alpha + A_3\alpha^2$; $C_L = B_1 + B_2\alpha + B_3\alpha^2$; ($\alpha$ in degree)

Mach	A_1	A_2	A_3	B_1	B_2	B_3
1.5	0.0380	-.000496	.000765	.00565	0.0431	-.000110
2	0.0335	-.000718	.000664	.00102	0.0363	-.000075
3	0.0250	-.001238	.000569	-.00285	0.0271	.000029
4	0.0211	-.001900	.000576	-.00832	0.0228	.000141
7.1	0.0201	-.002130	.000500	-.00245	0.0120	.000440
10*)	0.0200	-.002200	.000500	-.00245	0.0085	.000440
12*)	0.0200	-.002250	.000500	-.00245	0.0080	.000440

*) COEFFICIENTS GAINED BY EXTRAPOLATION

2) This value differs from the one given in ref. (1) because of the different value of constant dynamic pressure used in this paper. For Q = 100 kpa (as used in ref.1) the initial altitude would be 1760 m

The initial values for the angle of attack and thrust are:

$\alpha_I = 1.53$ deg

$T_I = 2366$ kN

The system of differential equations (eqn. (1), (2) and (4)) was solved by a Runge-Kutta-Fehlberg method (ref. 7). Fig. 4 (a)-(g) shows the result of the trajectory computation (phase 2) in various state- and system variables.

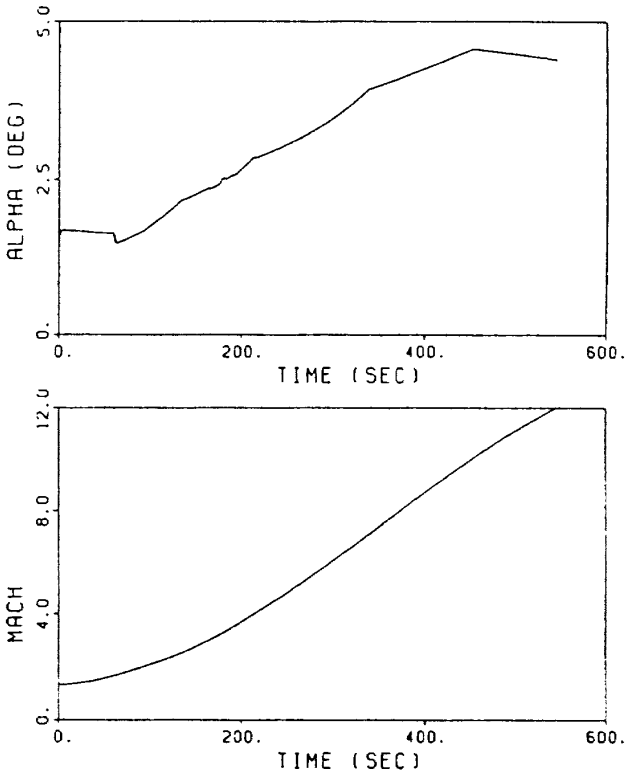

(b) Mach Nunber, angle of attack

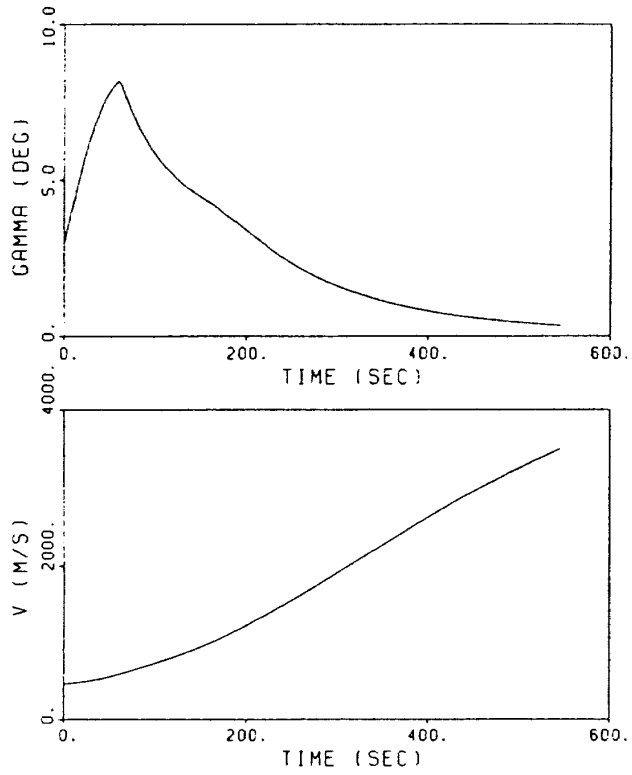

Fig 4. Ascent trajectory simulations results
(a) Flight velocity, climb angle

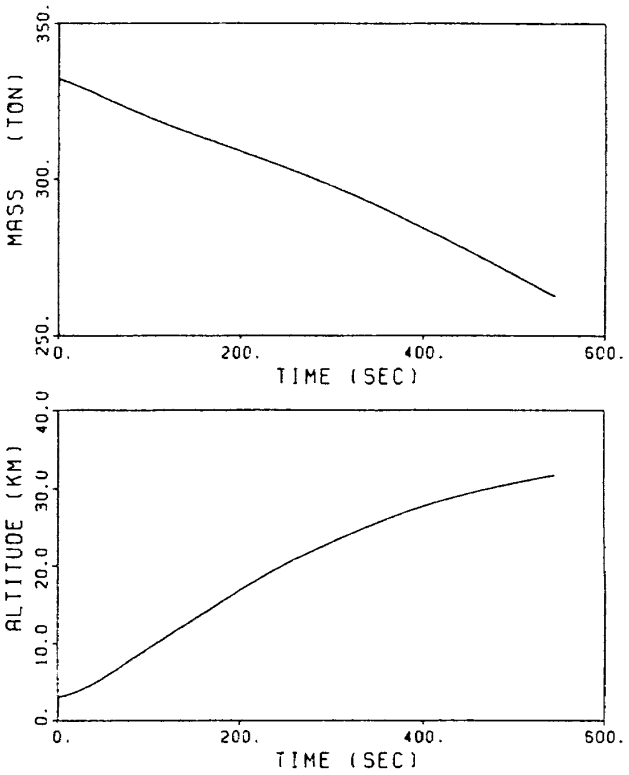

(c) Altitude, Spaceplane mass

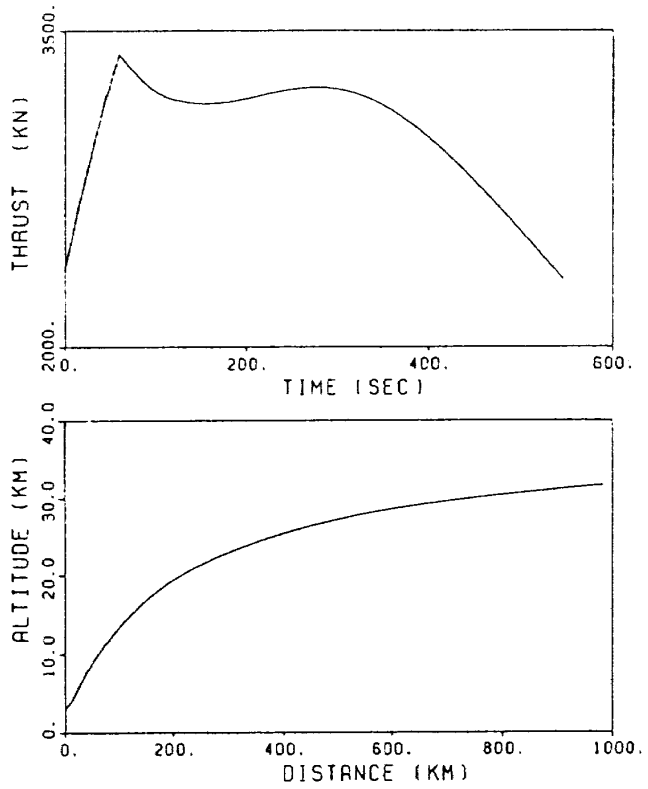

(d) Altitude vs. distance, thrust

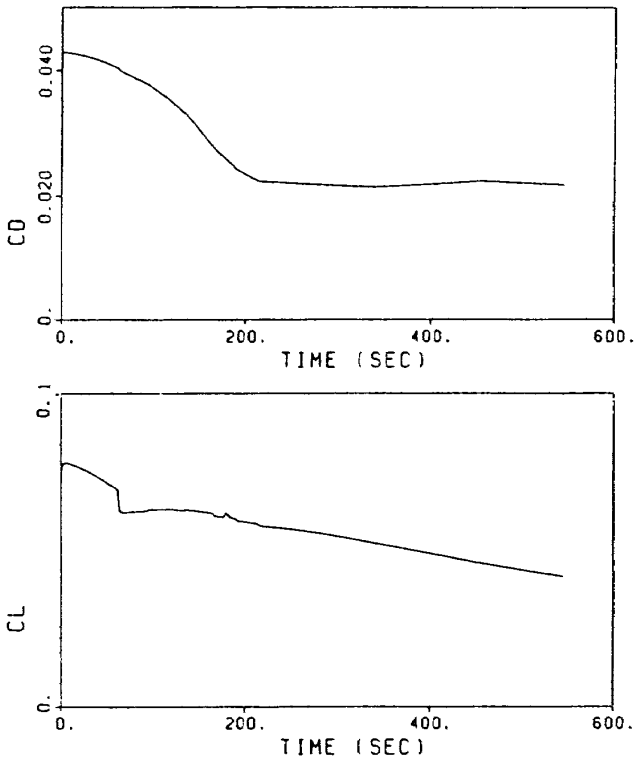

(f) Lift and drag coefficient

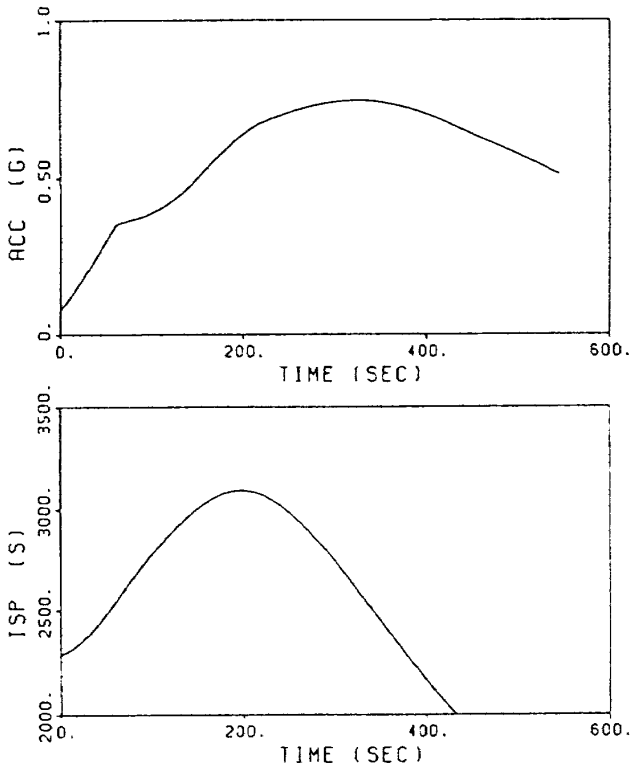

(e) Specific impulse, acceleration along flight path

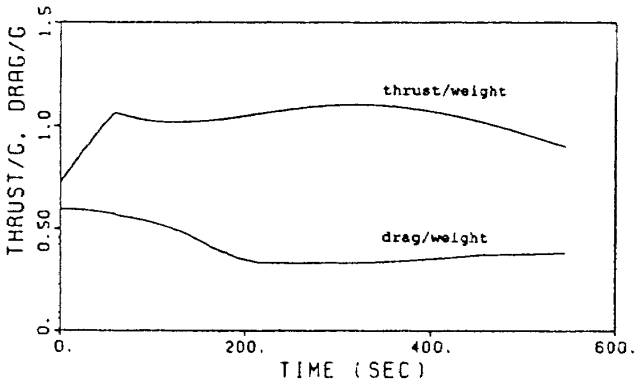

(g) Thrust/weight, drag/weight

4. DYNAMIC STABILITY OF UNAUGMENTED SPACEPLANE DURING SUPERSONIC AND HYPERSONIC ASCENT ALONG REFERENCE TRAJECTORY

4. 1 Method of analysis

In this paper the dynamic stability is described by the eigenvalues of the characteristic motions due to small perturbations from seven reference points defined on the above described reference trajectory at the Mach numbers M = 1.5, 2, 3, 4, 7.1, 10 and 12.[3]

Assuming a flat earth model and neglecting the time dependency of Spaceplane's mass and moments of inertia[4], the equations of motion describing the flight attitude of the rigid Spaceplane at each reference point are:

$$\dot{\alpha} = q - (p\cos\alpha + r\sin\alpha)\tan\beta + (\cos\alpha/mu)\,(F_z\cos\alpha - F_x\sin\alpha)$$

$$\dot{\beta} = p\sin\alpha - r\cos\alpha + (\cos\alpha\cos\beta/mu)\,(F_y\cos\beta - F_x\cos\alpha\sin\beta - F_z\sin\alpha\sin\beta)$$

$$\dot{u} = F_x/m - (qu\tan\alpha - ru\tan\beta/\cos\alpha)$$

$$\{\dot{\Omega}\}_b = [I]^{-1}\left(\{M\}_b - \{\Omega\}_b \times [I]\{\Omega\}_b\right)$$

$$\dot{\Phi} = p + q\sin\Phi\tan\theta + r\cos\Phi\tan\theta$$

$$\dot{\theta} = q\cos\Phi - r\sin\Phi \qquad (16)$$

The index 'b' indicates the bodyfixed coordinate system. u is the velocity component in bodyfixed w-direction and β is the angle of sideslip. $\{\Omega\}_b$ is the vector of angular velocities with the components: roll-rate (p), pitch-rate (q) and yaw-rate (r). Φ is the bank angle, θ is the pitch angle (for definition of the angular velocities and the bank- and pitch-angle, see fig. 5).

[I] is the matrix of Spaceplane's moments of inertia with respect to the body-fixed coordinate system.

The moments of inertia at the different reference points are gained from a linear interpolation between the values assumed for the take-off- and landing-condition (ref. 3).

F_x, F_y and F_z are the forces in direction of the body-fixed axis including aerodynamic forces, thrust and gravity forces. $(M)_b$ is the vector of aerodynamic moments with respect to the body-fixed axis consisting of the components: rolling moment (L), pitching moment (M) and yawing moment (N). The formulas for the forces and moments are:

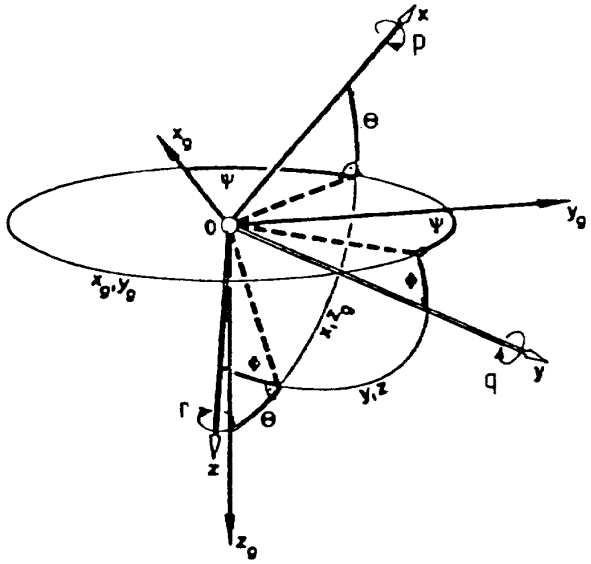

Fig. 5. Definition of angular velocities and rotation angles

3) The reference point Mach numbers M=1.5 to M=7.1 correnspond to the Mach numbers investigated in the windtunnel.

4) This simplification is justified because the time constants of the regarded characteristic motions are small compared with the time constants of the change in mass and moments of inertia.

$$
\begin{aligned}
F_x &= QSC_X - mg\sin\theta\cos\Phi + T \\
F_y &= QSC_Y + mg\sin\Phi \\
F_z &= QSC_z + mg\cos\theta\cos\Phi \qquad (17) \\
L &= QSbC_l \\
M &= QScC_m \\
N &= QSbC_n
\end{aligned}
$$

Q is the dynamic pressure, S the wing reference area, c the mean aerodynamic chord and b the wing-span. T is assumed to be aligned with the body-fixed x-axis.

The set of non-linear equations of motion (eqn. (16)) was linearized at the above mentioned non-equilibrium reference points[5] (accelerated flight during ascent) by application of the small-perturbation method (see for ex. ref. 12).

In the proximity of any reference point, the aerodynamic coefficients C_X, C_Y, C_Z, C_l, C_m and C_n are represented by the following perturbation series:

$$
\begin{aligned}
C_X &= C_{X,0} + C_{X\alpha}\,\Delta\alpha + C_{Xq}\,\Delta q \\
C_Y &= C_{Y,0} + C_{Y\beta}\,\Delta\beta + C_{Yp}\,\Delta p + C_{Yr}\,\Delta r + C_{Y\delta a}\,\Delta\delta_a \\
&\quad + C_{Y\delta r}\,\Delta\delta_r \\
C_Z &= C_{z,0} + C_{Z\alpha}\Delta\alpha + C_{Z\dot\alpha}\,\Delta\dot\alpha + C_{Zq}\,\Delta q + C_{Z\delta e}\,\Delta\delta_e \\
C_l &= C_{l,0} + C_{l\beta}\,\Delta\beta + C_{lp}\,\Delta p + C_{lr}\,\Delta r \\
&\quad + C_{l\delta a}\,\Delta\delta_a + C_{l\delta r}\,\Delta\delta_r \qquad (18) \\
C_m &= C_{m,0} + C_{m\alpha}\,\Delta\alpha + C_{m\dot\alpha}\,\Delta\dot\alpha + C_{mq}\,\Delta q \\
&\quad + C_{m\delta e}\,\Delta\delta_e \\
C_n &= C_{n,0} + C_{n\beta}\,\Delta\beta + C_{np}\,\Delta p + C_{nr}\,\Delta r \\
&\quad + C_{n\delta a}\,\Delta\delta_a + C_{n\delta r}\,\Delta\delta_r
\end{aligned}
$$

The index 0 indicates the value at the reference point and the letter $\triangle$ the perturbation form this reference point.

The complete sets of aerodynamic derivatives for each reference point together with the system- and state variables defining the non-equilibrium reference conditions are given in appendix 1.

The static aerodynamic derivatives at the considered seven reference points are derived form the above mentioned windtunnel tests (ref. 2 and unpublished NAL data) and were extrapolated for the Mach numbers 10 and 12.

The rotary derivatives are computed by application of *piston Theory* (ref. 8) to a three dimensional panel model of Spaceplane geometry (see appendix 2).

The $\dot\alpha$ -derivatives considered in eqn. (18) in formulas for C_z and C_m are estimated by approximating Spaceplane by a delta-wing and applying a simple formula given in ref. 9 based on potential theory.

The control derivatives for the elevator are derived from windtunnel measurements available up to Mach 7.1 and are extrapolated for the Mach numbers 10 and 12. for the aileron-and rudder-derivatives at supersonic and hypersonic speeds, measured data for Spaceplane were not available. Therefore, as a rough approximation, aileron- and rudder derivatives of the HIMES research model (ref. 10,11) (see fig. 6) are used, which have been measured up to a Mach number of 5. These values were inter- and

5) The application of the small-perturbation method is not restricted to equilibrium reference conditions.

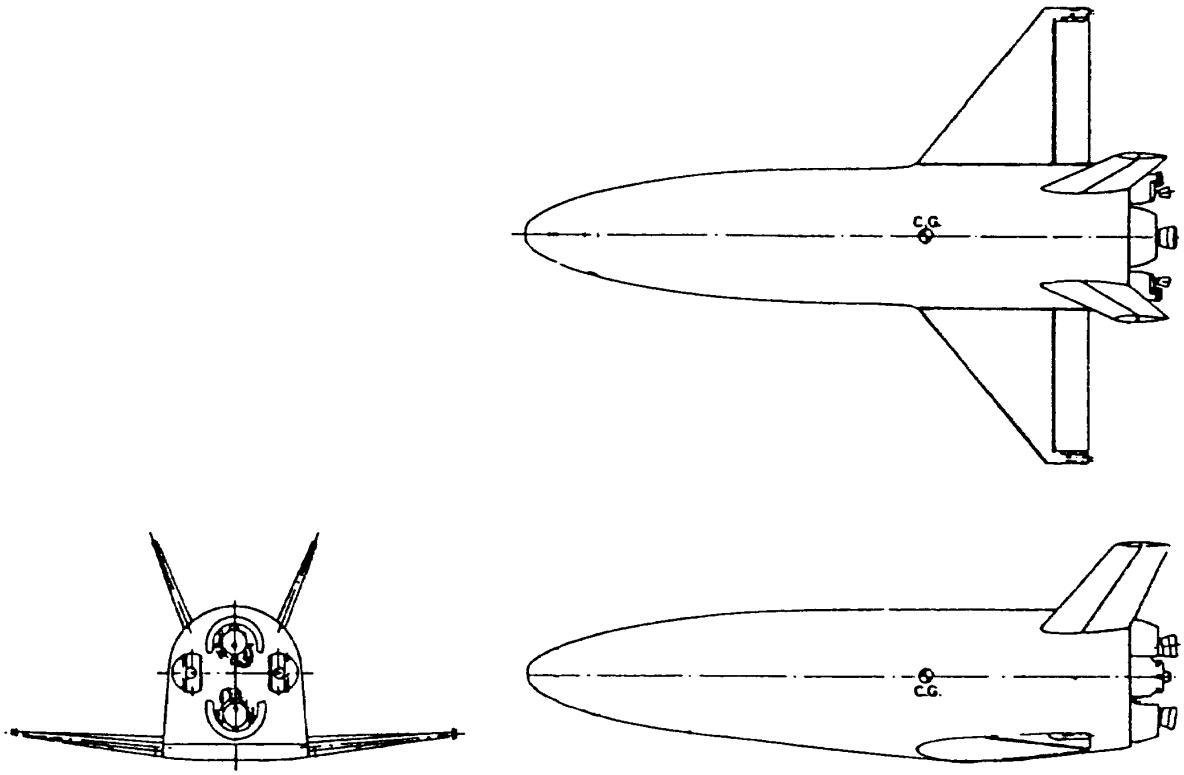

Fig. 6. Geometry of HIMES research model

extrapolated for the purpose of this paper.

The control-derivatives are not used in the unaugmented stability analysis but will be necessary later for the design of stability augmentation.

Finally, the linearization leads to the following set of linear e.o.m.:

$$\{\dot{x}\} = [A]\{x\} + [B]\{\delta\} \qquad (19)$$

where {X} is the vector of perturbations from the reference point state variables:

$$\{x\}^T = \{\Delta\alpha,\ \Delta\beta,\ \Delta u,\ \Delta p,\ \Delta q,\ \Delta r,\ \Delta\theta,\ \Delta\Phi\} \qquad (20)$$

and $\{\delta\}$ is the vector of the perturbations of the control variables from their condition at the reference point. $\{\delta\}$ consist of the perturbation deflections of the elevon ($\triangle\delta_e$), aileron ($\triangle\delta_a$) and rudder ($\triangle\delta_r$) and of the perturbation of thrust T:

$$\{\delta\}^T = \{\Delta\delta_e, \Delta\delta_a, \Delta\delta_r, \Delta T\} \qquad (21)$$

[A] is the characteristic system matrix and [B] is the control matrix. The eigenvalues of the matrix [A] in eqn. (19) describe the dynamic stability of the characteristic motions (see for ex. ref. 12), which are:

- short period motion
- phugoid motion

} longitudinal characteristic motions

- dutch-roll motion
- roll-motion
- spiral motion

} lateral characteristic motions

Because of the symmetric reference conditions ($\beta = 0$) assumed in this paper and because of the absence of coupling terms in the expressions for the aerodynamic forces and moments and in the inertia matrix [I],longitudinal and lateral characteristic motions can be treated

separately.

4. 2 Unaugmented stability results

Fig. 7 shows the eigenvalues of the characteristic longitudinal and lateral motions at the regarded reference points. The conjugate complex eigenvalue ω consisting of a real part (Re) and an imaginary part (Im), ω = Re ± i Im, can be expressed by a undamped natural frequency ω_0 and a damping coefficient ζ by employing the following relation:

$$\omega = -\zeta\omega_0 \pm i\omega_0\sqrt{1-\zeta^2}$$

$$\omega_0 = \sqrt{Re^2 + Im^2},$$

$$\zeta = \frac{-Re}{\sqrt{Re^2 + Im^2}}$$

a real eigenvalue (Re) may be expressed by a time constant T by use of :

$$T = 1/Re$$

Within the stepsize of the considered reference Mach numbers, for M>3 the short period solution has a component with positive real part because of the static longitudinal instability ($C_{m\alpha} > 0$). For the Mach numbers 7.1, 10 and 12, negative directional stability $C_{n\beta}$ leads to an unstable and non-oscillatory dutch-roll motion and to an unstable spiral mode.

The influence of the canard on the short period and phugoid eigenvalues is shown for the Mach numbers 1.5, 2, 3 and 4. Because of the

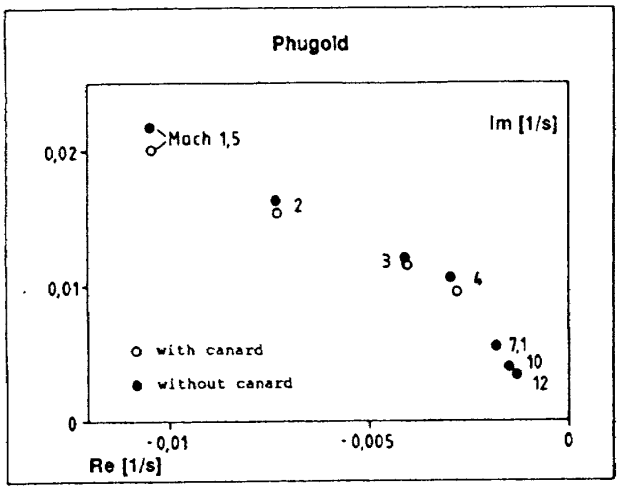

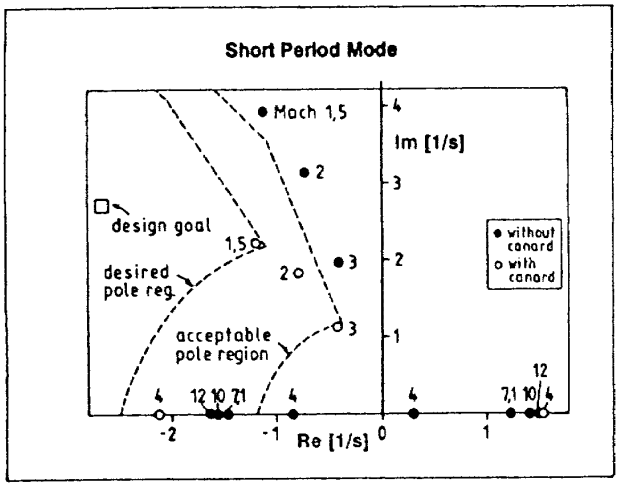

Fig. 7. Unaugmented stability results
(a) Phugoid, short period mode

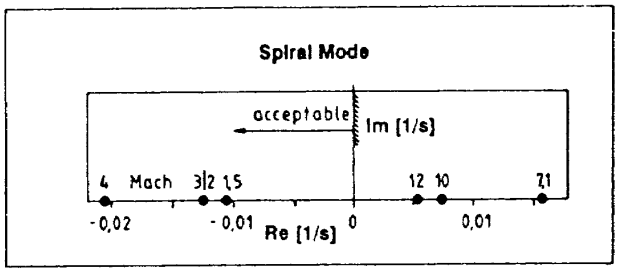

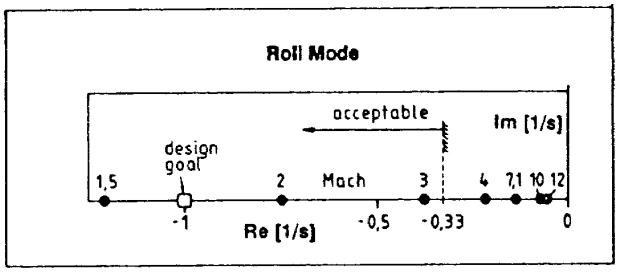

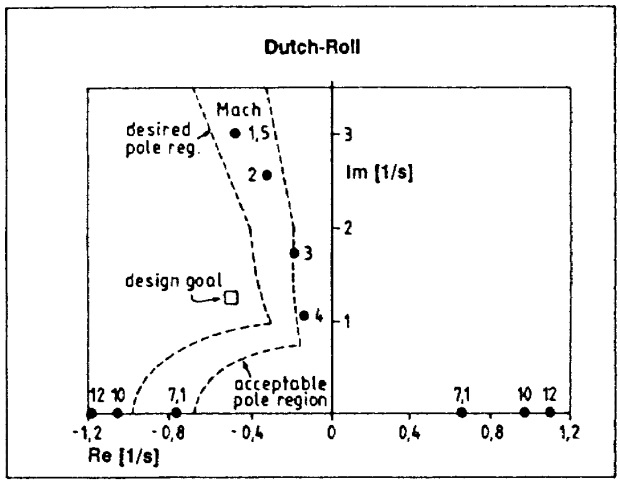

(b) Spiral mode, roll mode, dutch-roll

location of the canards far in front of the center of gravity and for the canard-setting assumed during the windtunnel tests (2° inclination to the body-fixed x-axis in the sense of producing a pitch-up moment) the canards lead to a decrease in the longitudinal static stability (shift of $C_{m\alpha}$ to positive values). Consequently the short period frequency is considerably lower than for the Spaceplane without canards. The slight increase of short period damping is due to the small increase of pitch-damping C_{mq}. The calculations show that the influence of the canards on the lateral stability can be neglected despite a small increase in the amount of roll-damping C_{lp} and rolling-moment due to sideslip $C_{l\beta}$.

5. STABILITY AUGMENTATION

In order to achieve a stable flight of Spaceplane during the whole considered ascent phase an output feedback control system is implemented. In contrast to a complete state feedback, output feedback means the feedback of not all but only a few selected state variables. The determination of the feedback gain constants is done in two steps. In the first step the eigenvalues of the characteristic system matrix are assigned to fixed pole locations within a region of the complex plane marked 'desired'. In the second step locations of poles within a region marked only 'acceptable' are regarded sufficient. The additional freedom in control design in the second step approach, resulting from allowing the poles to lay within a region of the complex plane rather than demanding a fixed location like in the first step, is used to minimize the sum of squares of the feedback gain constants to achieve low control surface deflections. The definition of the ratings 'desired' and 'acceptable' for Spaceplane handling is based on common handling quality criteria given in the literature (ref. 13, 14, 15).

Because of the assumption (eqn. (18)) that the control surfaces only have effect either on the longitudinal motion (elevator) or on the lateral motion (rudder, aileron), that means there is no coupling stipulated by the control system, longitudinal and lateral motion again can be treated separately.

The dynamic behaviour of the control surface actuators is neglected for simplicity.

Only Spaceplane configuration without canards is considered in the following investigation.

5. 1 Longitudinal motion stability augmentation

The angle of attack and pitch rate are fed back to control the elevator:

$$\Delta\delta_e = K_1 \Delta\alpha + K_2 \Delta q \qquad (22)$$

Because of the number of fed back state variables is two, only one of the two conjugate complex poles (short period or phugoid) can be assigned.

Because the dynamics of the longitudinal motion is dominated by the short period motion which also is the critical one due to its natural instability at high Mach numbers, the eigenvalues of the short period motion were assigned.

In the first design approach ('step 1') the feed back gains are computed to achieve desired eigenvalues ('design goal' in fig. 7a) according to handling quality criteria given in ref. 13.

The desired location of the pole of the short period motion (index: S.P.) in the complex plane is ($i = \sqrt{-1}$):

$$\omega_{S.P.} = -2.660 \pm i\, 2.713\ (\mathrm{sec}^{-1})$$

Fig. 8 shows the results for the gain constants K_1 and K_2 for this design for the seven reference Mach numbers. With increasing

instability of the unaugmented Spaceplane the amount of stabilizing input, i.e. the amount of the feedback gain constants, increases. In order to alleviate the amount of the gain constants and so to decrease the corresponding elevator deflection, in the second design approach ('step 2') any location of the short period eigenvalues within the region of the complex plane marked 'acceptable' (bounded by a dashed line in fig. 7a) was allowed but additionaly it was demanded to minimize the sum of squares of the gain constants:

$$\sqrt{K_1^2 + K_2^2} \rightarrow \mathrm{Min}$$

The resulting gain constants are shown with dashed lines in fig. 8. To obtain a feeling for what the magnitude of the gain constants means, fig. 9 shows for the seven reference Mach numbers the controlled elevator deflection amplitude which would occur during a short period motion with an angle of attack amplitude of 1° (solid line: 'step 1', dashed line: 'step 2'). The elevator deflection amplitude is thereby computed by the formula:

$$| \delta_e | = | \{ K_1, K_2, 0, 0 \}^T \{ x \}_{S.P.} | \tag{23}$$

where $\{x\}_{S.P.}$ is the complex eigenvector of the short period motion consisting of the elements $\{ \Delta\alpha, \Delta q, \Delta u, \Delta\theta \}$ normalized so that $\Delta\alpha$ is 1°.

Although the high elevator deflections at high Mach numbers might worry, an ascent simulation in clear air turbulence, carried out later in this paper, shows, that the elevator deflection

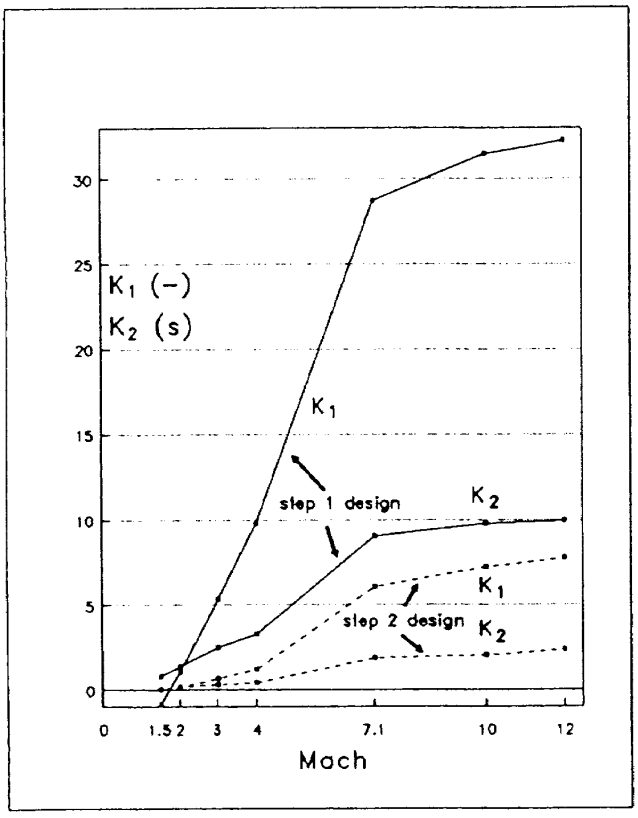

Fig. 8. Feedback gain constants-longitudinal motion-feedback to elevator

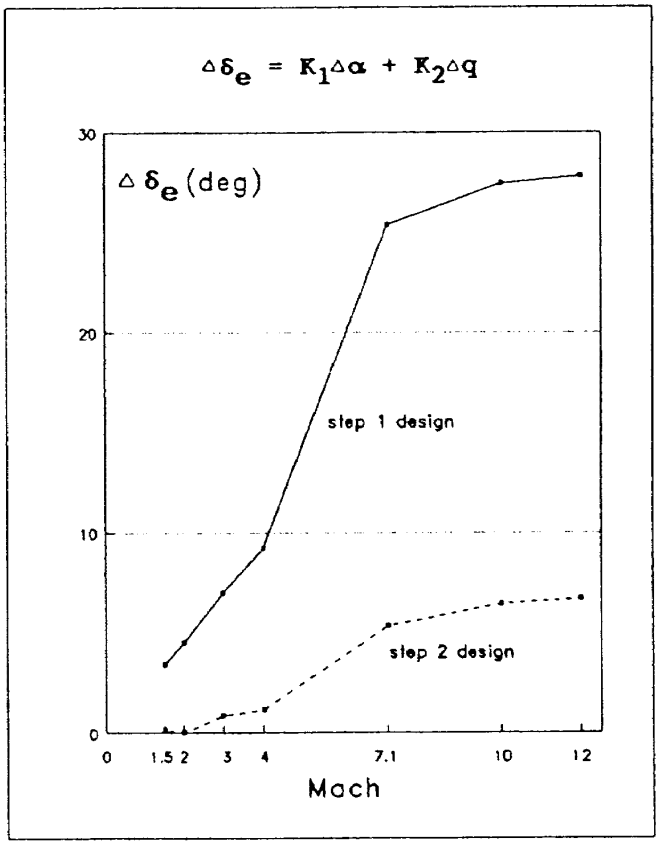

Fig. 9. Controled elevator deflect for short period motion of 1 deg amplitude in angle of attack

amplitudes to be expected during Spaceplane super- and hypersonic ascent have a reasonable magnitude.

The phugoid eigenvalues for the "step 1" and the short period and phugoid eigenvalues for the "step 2" are shown in Table 2 and 3 respectively.

In the 'step 2' design the phugoid becomes a non-oscillatory motion with a weak unstable part for the Mach numbers 7.1, 10 and 12.

The conputation of the gain constants for both design steps was carried out using the FACOM program library (ref. 16) minimization routine MINF1. The costfunction minimized in the 'step 1'-design was the distance of the short period eigenvalue from the design goal, in the 'step 2' — design the sum of squares of the gain constants superimposing an error if the eigenvalue was located outside the acceptable pole region.

Table 2 The phugoid eigenvalues for the first design approach (step 1)

Mach	phugoid [sec^{-1}]
1.5	$-0.11\cdot10^{-1} \pm i\ 0.22\cdot10^{-1}$
2.	$-0.73\cdot10^{-2} \pm i\ 0.15\cdot10^{-1}$
3.	$-0.39\cdot10^{-2} \pm i\ 0.94\cdot10^{-2}$
4.	$-0.25\cdot10^{-2} \pm i\ 0.59\cdot10^{-2}$
7.1	$-0.38\cdot10^{-2} \pm i\ 0.34\cdot10^{-2}$
10.	$-0.39\cdot10^{-2} \pm i\ 0.21\cdot10^{-2}$
12.	$-0.33\cdot10^{-2} \pm i\ 0.19\cdot10^{-2}$

5. 2 Robustness of the longitudinal motion control design

The sensitivity of the eigenvalue λ to a change in the feedback gain constants K_j, i.e. the robustness of the control design, can be obtained from the following expression (see ref.17):

$$d\lambda_i / dK_j = \frac{\underline{y}_i^T \left[dA/dK_j \right] \underline{x}_i}{\underline{y}_i^T \underline{x}_i} \qquad (24)$$

where $\underline{x}_i$ and $\underline{y}_i$ are the right and left eigenvector of the closed loop system matrix belonging to the eigenvalue λ_i and $[dA/dK_j]$ is the derivative of the closed loop system matrix [A] with respect to the gain constant K_j. When multiplying eqn. (24) with the factor K_j/λ_i one obtains the ratio of percentage change in the eigenvalue to the percentage change in the gain constant, called S subsequently:

$$S \equiv \frac{d\lambda_i / \lambda_i}{dK_j / K_j} \qquad (25)$$

If, for example, S = 0.7 then a 10% change in K_j leads to a 7% change in λ_i. In tab. 4 S is given for the 'step 1' and 'step 2' controller design and the Mach numbers 1.5, 3, 7.1 and 12.

Only in two cases S is significantly lager than 1. This occurs for the sensitivity of the short period imaginary part with respect to K_1 (corre-

Table 3 The short period and phugoid eigenvalues for the second design approach (step 2) (i = v−1)

Mach	short period [sec^{-1}]	phugoid [sec^{-1}]
1.5	$-1.18 \pm i\ 3.90$	$-0.11\cdot10^{-1} \pm i\ 0.22\cdot10^{-1}$
2.	$-0.74 \pm i\ 3.13$	$-0.74\cdot10^{-2} \pm i\ 0.16\cdot10^{-1}$
3.	$-0.69 \pm i\ 2.20$	$-0.41\cdot10^{-2} \pm i\ 0.11\cdot10^{-1}$
4.	$-0.58 \pm i\ 1.13$	$-0.24\cdot10^{-2} \pm i\ 0.48\cdot10^{-2}$
7.1	$-0.65 \pm i\ 1.08$	$-0.38\cdot10^{-2},\ +0.10\cdot10^{-2}$
10.	$-0.62 \pm i\ 1.09$	$-0.39\cdot10^{-2},\ +0.15\cdot10^{-2}$
12.	$-0.69 \pm i\ 1.06$	$-0.33\cdot10^{-2},\ +0.12\cdot10^{-2}$

sponds to $C_{m\alpha}$) at the Mach numbers 7.1 and 12 and for the 'step 2' −design.

The sensitivity analysis also gives information about the effect of the different feedback gain constants on the different characteristic modes of motion. It can be seen, that the real part of the short period eigenvalue (corresponding to the damping) is almost not sensitive to K_1. Except for the 'step 2' −design at high Mach numbers, the phugoid eigenvalues are almost not sensitive to changes in K_1 and K_2.

5. 3 Lateral motion stability augmentation

In the lateral motion, the roll-rate and bank angle are fed back to the aileron, the sideslip angle and yaw-rata to the rudder.

$$\Delta\delta_a = K_3\,\Delta p + K_4\,\Delta\Phi \tag{26}$$

$$\Delta\delta_r = K_5\,\Delta\beta + K_6\,\Delta r \tag{27}$$

That means, because of a feedback of all four state variables, all four pole locations can be assigned. analog to the control design for the longitudinal motion, a 'step 1' pole assignment towards fixed pole locations and a 'step 2' design aiming to minimize the feedback gain constants by allowing the eigenvalues to be located within a region of the complex plane marked 'acceptable', was carried out.

Desired and acceptable regions of the dutch-roll root locus are given in ref.13, 14. In the 'step 1' assignment the location marked 'design goal' in fig. 7 (b) is assigned.

The regions of desired and acceptable dutch-roll pole locations are marked with a dashed line in fig. 7 (b).

For the non-oscillatory rolling mode, recommended time constants for the rolling motion according to MIL-STD-1797 are given in ref.

Table 4 Sensitivities S of pole locations of longitudinal motion to changes in feedback gain constants.
Index : S. P. = short period, Ph = phugoid

	'step 1' design				'step 2' design			
Mach 1.5	$Re_{S.P.}$	$Im_{S.P.}$	Re_{Ph}	Im_{Ph}	$Re_{S.P.}$	$Im_{S.P.}$	Re_{Ph}	Im_{Ph}
K_1	-0.009	-0.22	0.010	0.044	-.0012	-0.007	0.0005	0.0023
K_2	0.587	-0.478	-0.003	-0.054	.078	-0.005	-.0002	-.0029
Mach 3	$Re_{S.P.}$	$Im_{S.P.}$	Re_{Ph}	Im_{Ph}	$Re_{S.P.}$	$Im_{S.P.}$	Re_{Ph}	Im_{Ph}
K_1	0.013	0.636	-0.014	-0.054	.006	0.121	-0.013	-0.046
K_2	0.834	-0.743	-0.003	-0.035	.407	-0.029	-0.002	-0.016
Mach 7.1	$Re_{S.P.}$	$Im_{S.P.}$	Re_{Ph}	Im_{Ph}	$Re_{S.P.}$	$Im_{S.P.}$	Re_{Ph}	Im_{Ph}
K_1	0.007	1.078	0.020	0.110	0.005	1.433	-2.065	-9.060
K_2	0.944	-0.890	-0.001	-0.001	0.800	-0.264	-0.004	-0.033
Mach 12	$Re_{S.P.}$	$Im_{S.P.}$	Re_{Ph}	Im_{Ph}	$Re_{S.P.}$	$Im_{S.P.}$	Re_{Ph}	Im_{Ph}
K_1	0.005	1.133	0.017	0.172	0.004	1.781	-1.507	-4.938
K_2	0.969	-0.921	-0.001	-0.007	0.894	-0.355	-0.004	-0.020

15. In 'step 1' a time constant of 1 sec was selected as design goal. A value of lower than 3 sec was regarded acceptable. Concerning the definition of a desired location of the spiral non-oscillatory root the relation of this pole location to the *Lateral Control Departure Parameter* LCDP (AADP), and the *Dynamic Directional Stability Parameter* $C_{n\beta,DYN}$, see for ex. Weissman (ref. 18), were regarded.

$$LCDP = C_{n\beta}{}^* - C_{l\beta}{}^* \frac{C_{n\delta a}}{C_{l\delta a}} \tag{28}$$

$$C_{n\beta,DYN} = C_{n\beta}{}^* \cos\alpha - \left(I_z / I_x\right) C_{l\beta}{}^* \sin\alpha \tag{29}$$

where $C_{n\beta}{}^*$ and $C_{l\beta}{}^*$ are the augmented yawing- respectively rolling-moment due to sideslip:

$$\text{where } C_{n\beta}{}^* = C_{n\beta} + K_5 C_{n\delta r} \tag{30}$$

$$\text{and } C_{l\beta}{}^* = C_{l\beta} + K_5 C_{l\delta r} \tag{31}$$

According to ref. 19, if both $C_{n\beta,DYN}$ is positive and LCDP is positive or greater than -0.0017 (deg^{-1}), ordinary control laws can be adopted for the lateral/directional flight control. LCDP less than -0.0017 (deg^{-1}) may lead to aileron reversal. A detailed discussion of these two parameters and their relation to flight dynamic behaviour is presented in ref. 19.

The relation of the two parameters $C_{n\beta,DYN}$ and LCDP to the spiral root locus of Spaceplane is shown in fig. 10 for the Mach numbers 1.5, 7.1 and 12. Fig. 10 results from computing LCDP and $C_{n\beta,DYN}$ for six different assignments of the spiral root while the root loci for the dutch-roll and the rolling motion are assigned to the design goals described above.

Fig. 10 shows, that even for an unstable (positive) spiral root of 0.05 sec^{-1} LCDP is greater than -0.0017 deg^{-1} for the three regarded Mach numbers. However, to provide a safe distance from this critical value, the design goal for the spiral root was set to -0.01 sec^{-1} for all Mach numbers, values lower than 0 were regarded acceptable.

Eqn. (28-31) show that the parameters $C_{n\beta,DYN}$ and LCDP are affected by only one gain constant, i.e. the gain constant for the feedback of the sideslip angle to the rudder, K_5.

Because the aileron derivative $C_{n\delta_a}$ is assumed to be zero in this investigation (see appendix 1), LCDP isdirectly proportional to the augmented directional stability $C_{n\beta}{}^*$.

The desired pole location for the dutch-roll (index:dr), roll motion (ro) and spiral motion (s) in the complex plane are:

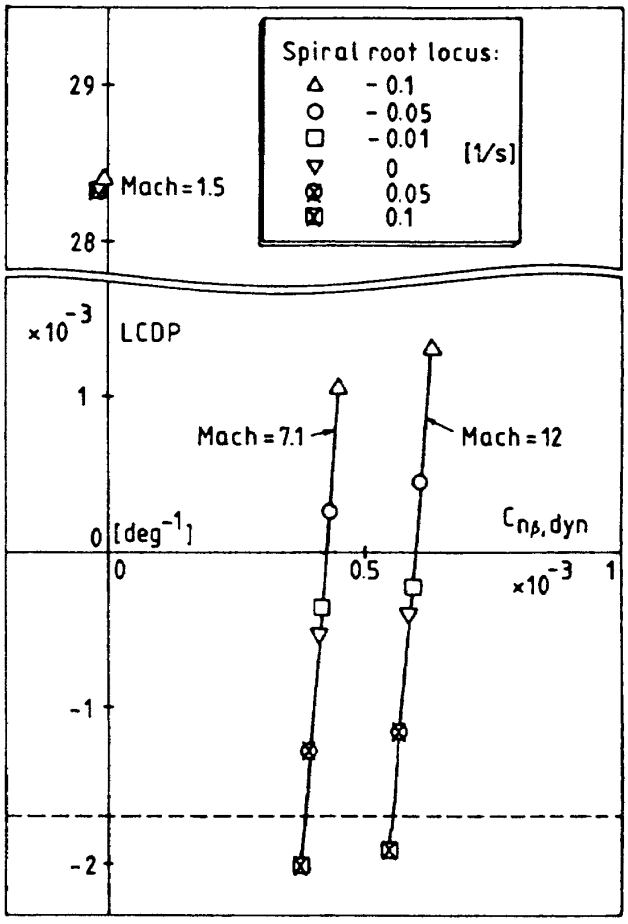

Fig. 10. LCDP vs. $C_{n\beta,dyn}$ for different spiral root assignments

dutch roll motion : $\omega_{dr} = -0.5 \pm i\ 1.25$ (sec^{-1})

roll motion : $\omega_{ro} = -1.0$ (sec^{-1})

spiral motion : $\omega_s = -0.01$ (sec^{-1})

In the 'step 1' -design, for the four desired pole locations specified, the solution for the corresponding four gain cnstants K_3 - K_6 were found by equating the coefficients of the characteristic equation of the augmented system matrix with the coefficients of the polynom gained by the product:

$$\Pi\ (\omega - \omega_{desired})$$

The system of the four algebraic equations was solved by the FACOM program library routine NOLBR (ref. 16). In the 'step 2' -design, the solution of the gain constants was found by employing a minimization routine described in ref. 20. Results for the gain constants are shown in fig. 11, dashed lines refer to the 'step 2' -design results begin at the Mach number 4 because for lower Mach numbers the eigenvalues of the unaugmented Spaceplane already are located within the acceptable region.

The corresponding maximum deflection angles of the aileron and rudder, during a dutch-roll motion with an angle of sideslip amplitude of 1°, can be seen in fig. 12.

While the controlled aileron defelection in the 'step 2' -design is significantly smaller than in the 'step 1' design, adplitude of the rudder deflection angle remains large. This can be explained by regarding the above discussion on the *Lateral Control Departure Parameter* LCDP. With eqn. (28) and (30) and $C_{n\delta_a} = 0$ follows:

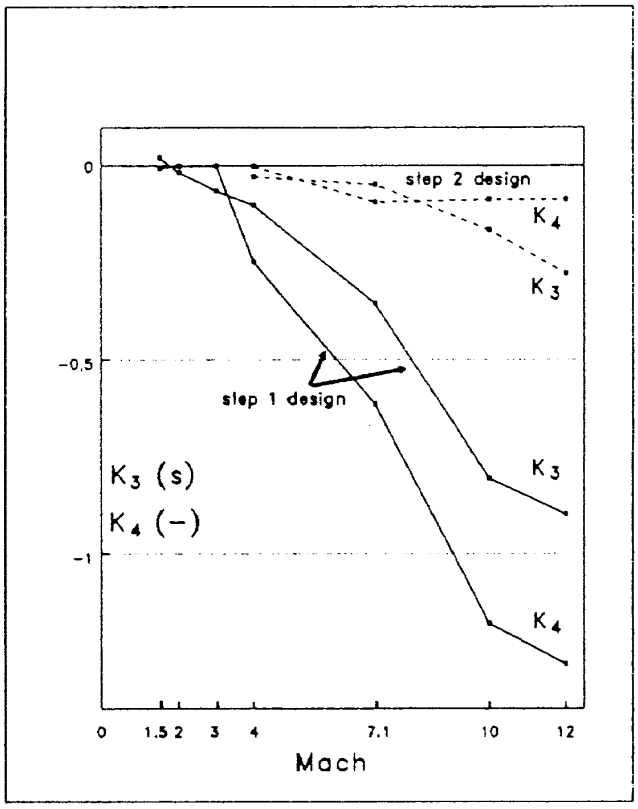

Fig. 11.Feedback gain constants-lateral motion
(a) feedback to aileron

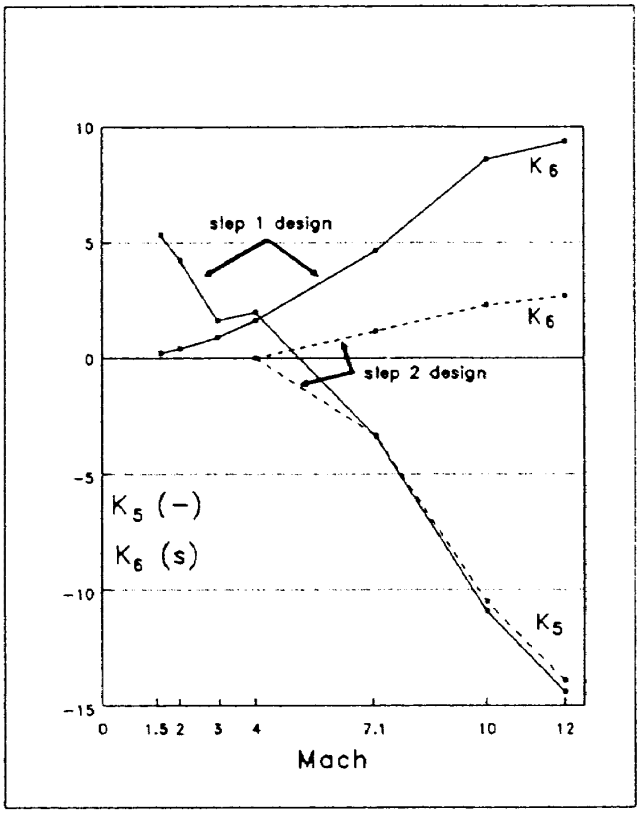

(b) feedback to rudder

$$C_{n\beta} + K_5 C_{n\delta r} = LCDP \geq -0.0017 \deg^{-1} \tag{32}$$

Eqn.(32) shows the dependency of K_5 on the aerodynamic derivatives $C_{n\beta}$ and $C_{n\delta r}$. An alleviation of K_5 can only be achieved by increasing the natural directional stability $C_{n\beta}$ or by increasing the rudder effectiveness $C_{n\delta r}$ for instance by use of a reaction control systems (RCS). Theis might be necessary especially at high Mach numbers where a severe decrease of rudder effectiveness occurs. A yaw control by purly aerodynamic means seems not to be sufficient in this flight regime.

Tabel 5 summarizes the closed pole for the "step 2" design.

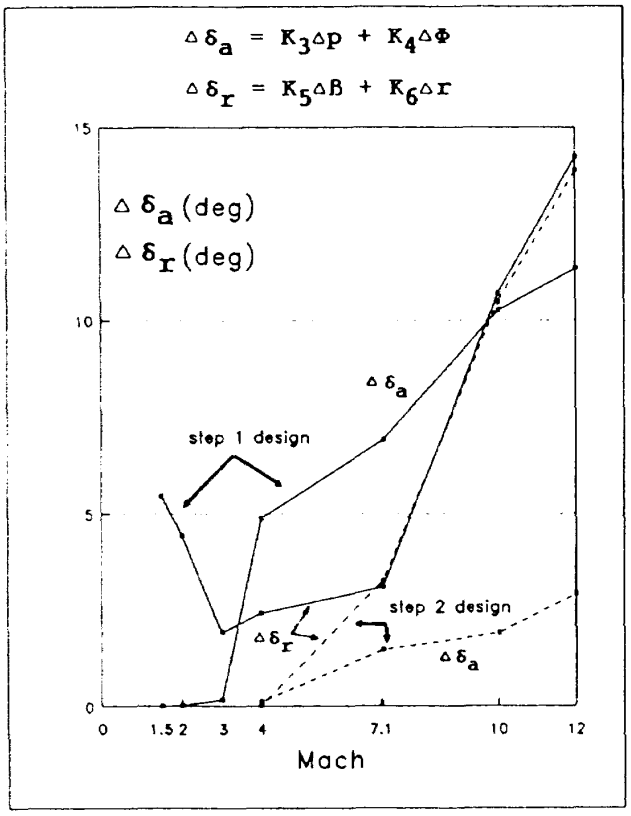

Fig. 12. Controled rudder and aileron deflections for dutch roll motion of 1 deg amplitude in sideslip angle

5. 4 Robustness of the lateral control

Analog to chapter 5.2, the sensitivity of the eigenvalues of the lateral motion to changes in the feedback-gain constants have been computed.

Results are given in tab.6. Except two cases, the sensitivities S (see eqn. (25)) of the dutch- roll and roll mode in the 'step 1' design are less than 1. The high sensitivities for the spiral root locus result from its proximity to the zero point in the complex plane. In this case a small absolute change in spiral root locus leads to a high percental change.

The sensitivity analysis also gives information about the influence of the different feedback gain constants on the different characteristic modes of motion. It can be seen that this influence is not the same for the different Mach numbers considered. For instance the feedback gain constant K_3 has almost no influence on the real part of the dutch roll eigenvalue at the Mach numbers 1.5 and 3 but a remarkable influence at the Mach numbers 7.1 and 12. One reason for that behaviour lies in the fact that the relation $K_3 : K_4 : K_5 : K_6$ of the feedback gain constants is not the same for the Mach numbers 1.5, 3 and 7.1. For the Mach

Table 5. The closed loop poles for the "step 2".

Mach	dutch-roll [sec^{-1}]	roll [sec^{-1}]	spiral [sec^{-1}]
4.	-0.162 ± i 1.035	-0.37	$-0.401 \cdot 10^{-1}$
7.1	-0.125 ± i 0.700	-0.33	$-0.614 \cdot 10^{-7}$
10.	-0.129 ± i 0.688	-0.33	$-0.469 \cdot 10^{-3}$
12.	-0.177 ± i 0.677	-0.34	$-0.212 \cdot 10^{-4}$

Table 6. Sensitivities S of pole locations of lateral motion to changes in feedback gain constants.

	'step 1' design				'step 2' design			
Mach 1.5	Re_{dr}	Im_{dr}	Re_{ro}	Re_s	Re_{dr}	Im_{dr}	Re_{ro}	Re_s
K_3	0.010	0.006	0.384	0.498	-	-	-	-
K_4	0.001	0.001	0.048	4.90	-	-	-	-
K_5	-0.840	2.184	0.974	23.8	-	-	-	-
K_6	0.281	0.054	0.026	1.843	-	-	-	-
Mach 3	Re_{dr}	Im_{dr}	Re_{ro}	Re_s	Re_{dr}	Im_{dr}	Re_{ro}	Re_s
K_3	0.015	-0.023	0.652	-0.680	-	-	-	-
K_4	0.	0.	-0.006	0.588	-	-	-	-
K_5	-0.029	-0.376	0.019	0 .	-	-	-	-
K_6	0.598	-0.081	-0.013	0.	-	-	-	-
Mach 7.1	Re_{dr}	Im_{dr}	Re_{ro}	Re_s	Re_{dr}	Im_{dr}	Re_{ro}	Re_s [1)]
K_3	0.890	-0.144	-0.003	0.	0.507	-0.015	-0.021	0.002
K_4	0.004	0.494	0.005	-0.94	-0.018	0.256	0.129	-0.402
K_5	0.076	0.066	-0.630	55.5	0.561	0.458	-3.190	0.273
K_6	-0.024	-0.002	0.887	2.08	-0.088	-0.009	0.634	-0.030
Mach 12	Re_{dr}	Im_{dr}	Re_{ro}	Re_s	Re_{dr}	Im_{dr}	Re_{ro}	Re_s [1)]
K_3	0.955	-0.153	-0.004	0.	0.940	-0.062	-0.112	.0001
K_4	0.002	0.436	0.006	-0.707	-0.004	0.114	0.104	-.390
K_5	0.176	0.193	-1.263	108.7	0.494	1.540	-2.787	.0556
K_6	-0.014	-0.001	0.933	1.19	-0.130	-0.002	0.836	-.0114

1) because the spiral root locus is almost zero, instead of $(d\lambda/\lambda)/(dK_j/K_j)$ the value of $d\lambda/dK_j$ is given

number 12 the relation is similar to the one at Mach 7.1, therefore at these two Mach numbers the sensitivities of the eigenvalues to changes in the feedback constants possess the same tendency.

For the 'step 2'design the sensitivities are slightly higher than for the 'step 1' design.

6. SIMULATION OF AUGMENTED SPACEPLANE ASCENT IN DISTURBED ATMOSPHERE (motion in the longitudinal plane)

The super- and hypersonic atmospheric ascent is simulated considering three degrees of freedom motion in the longitudinal plane. The simulation is divided into two parts, which are dependent on each other. First, Spaceplane's vehicle dynamics is represented by the system matrices at the seven reference Mach numbers used in the stability analysis (Spaceplane configuration without canards). The linear output feedback control using the feedback gains from the 'step 1' control design shown in fig.8 are incorporated. The feedback gains and system matrices for any Mach number are found by linear interpolation between the values

for the reference Mach numbers.

Second, the trajectory control itself, i.e. the control of the constant dynamic pressure Q, is achieved by a linear feedback of the deviation of the dynamic pressure Q from its desired value Q_0 (85 kPa) to generate a commanded angle of attack α_c.

$$\alpha_C = K\,(Q_0 - Q) + \alpha_{M=1.33} \qquad (33)$$

$\alpha_{M=1.33}$ is the angle of attack at the beginning of the considered ascent trajectory phase where Mach number M=1.33 and $Q=Q_0$. Because of the simple controller design of only proportional type, a deviation of the dynamic pressure Q from the desired value Q_0 is unavoidable. The stability analysis of this trajectory control and the determination of the factor K in eqn. (33) is described in appendix 3. The factor K depends on the Mach number and takes the following values:

Mach	K [deg/kPa]
1.5	.29
2	.47
3	.71
4	.95
7.1	1.25
10	1.33
12	1.70

The vehicle is assumed to be trimmed at the commanded angle of attack α_C.[6)]

The ascent simulation considers the effect of vertical gustvelocities w_{turb} (frozen gust model) occuring during standard clear air turbulence. The magnitude and sign of the vertical gust velocity w_{turb} is given by a random number with a root-mean-square intensity according to USAF MIL Spec.8785 (ref.21, see fig.13). The duration while w_{turb} is kept constant is defined by the actual flight velocity and by altitude dependent horizontal scales of the gust model as given in ref.22. The additional, disturbing angle of attack due to clear air turbulence is approximated by:

$$\Delta\alpha_{\text{turb}} \cong w_{\text{turb}}/V \qquad (34)$$

The equations of motion employed in the trajectory simulation consist of the small perturbation equations or the rigid body dynamics:

$$\{\dot{\Delta x}\} = [A]\{\Delta x\} + \{b\}\Delta\delta_e + \{c\}\Delta\alpha_{\text{turb}} \qquad (35)$$

$$\{\Delta x\}^T = \{\Delta\alpha,\ \Delta q,\ \Delta u,\ \Delta\theta\} \qquad (36)$$

$$\Delta\delta_e = K_1\Delta\alpha + K_2\Delta q \qquad (22)$$

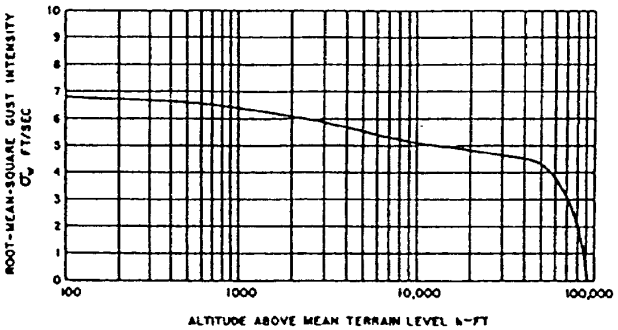

Fig. 13. Intensity of clear air turbulence (USAF MIL Spec. 8785)

6) For the elevator deflection $\delta_{e,\,trim}$ necessary to trim Spaceplane, see appendix 1. The trim capability of the elevator might be augmented by bodyflap or center of gravity. The different sign in $C_{m,\,0}$ and $\delta_{e,\,trim}$ for Spaceplane with (δc = 2 deg) and without canards result from the location of the neutral point before (with canard) or behind (without canard) the center of gravity (68% length from nose).

$$\{c\}^T = \left\{ \frac{QSC_{L\alpha}}{mV}, \frac{QScC_{m\alpha}}{I_{YY}}, \frac{QSC_{X\alpha}}{m}, 0 \right\} \quad (37)$$

and of equations for the trajectory dynamics, considering Spaceplane as a mass point:

$$\dot{v}_0 = \frac{T(h,M)}{m}\cos\alpha - g\sin\nu - \frac{Q}{m}SC_D(\alpha^*, M) \quad (38)$$

$$\dot{\nu}_0 = \frac{T(h,M)}{mV}\sin\alpha - \frac{g}{V}\cos\nu + \frac{V}{R}\cos\nu + \frac{Q}{mV}SC_L(\alpha^*, M) \quad (39)$$

$$\dot{Q} = -\frac{V}{h_s}Q\sin\nu + \rho\dot{V}V_0 \quad (3)$$

$$\dot{m} = -\frac{T(h,M)}{I_{SP}\,g} \quad (4)$$

$$\dot{h} = V\sin\nu \quad (40)$$

The index '0' indicates that the respective variable describes the reference condition.

The state variables α, α^*, ν, V and Q are defined as follows:

$$\alpha = \alpha_C + \Delta\alpha \quad (41)$$

$$\alpha^* = \alpha + \Delta\alpha_{\text{turb}} \quad (42)$$

$$\nu = \nu_0 + \Delta\theta - \Delta\alpha \quad (43)$$

$$V = V_0 + \Delta u/\cos\alpha \quad (44)$$

$$Q = 1/2\,\rho V^2 \quad (8)$$

The system of differential equations was solved by a Runge-Kutta-Fehlberg method (ref.7). The initial conditions are those given in chapters 3.2 and 3.3 and moreover:

$$\{\Delta x\}_I = 0 \quad (45)$$

Fig.14 shows time histories of the state variables, the elevator deflection $\Delta\delta_e$, the additional angle of attack α_{turb} due to the air turbulence and the Mach number M. The elevator deflection angle does not include the portion needed to trim Spaceplane at the commanded angle of attack. The dashed lines indicate the reference trajectory computed without consideration of vehicle dynamics and atmospheric guests in the same way as chapter 3.3.

The results show that the ascent is dynamically stable and that the elevator deflection angles necessary to counteract the disturbances

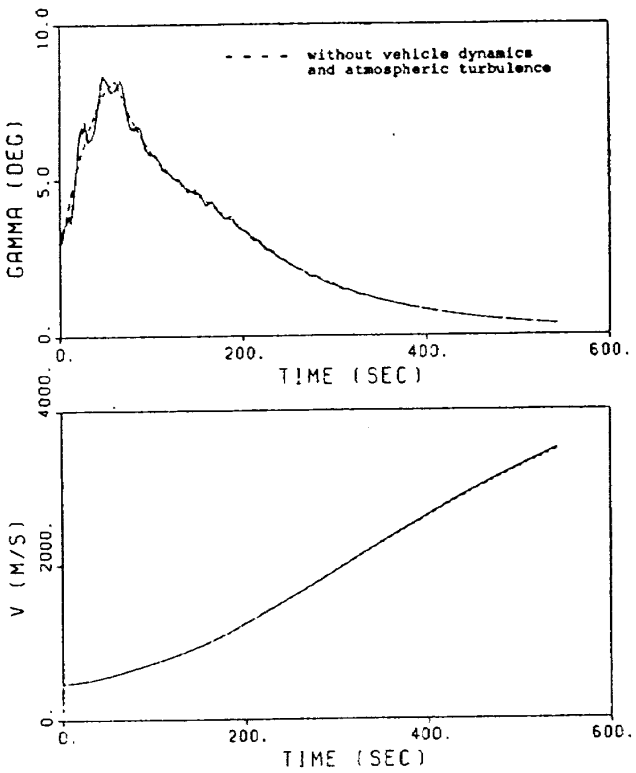

Fig. 14. Ascent trajectory simulation results (under consideration of vehicle dynamic and atmospheric turbulence)
(a) Flight velocity, climb angle

due to the clear air turbulence are small (less than 0.3 degrees). The elevator deflections remain small even at high Mach numbers where the feedback gain constants are large. This can be explained by the negligible small disturbing angle of attack due to clear air turbulence in the high altitude, high speed trajectory phase.

The maximum deviation of the dynamic pressure from the reference value of 85 kPa is only about 1%.

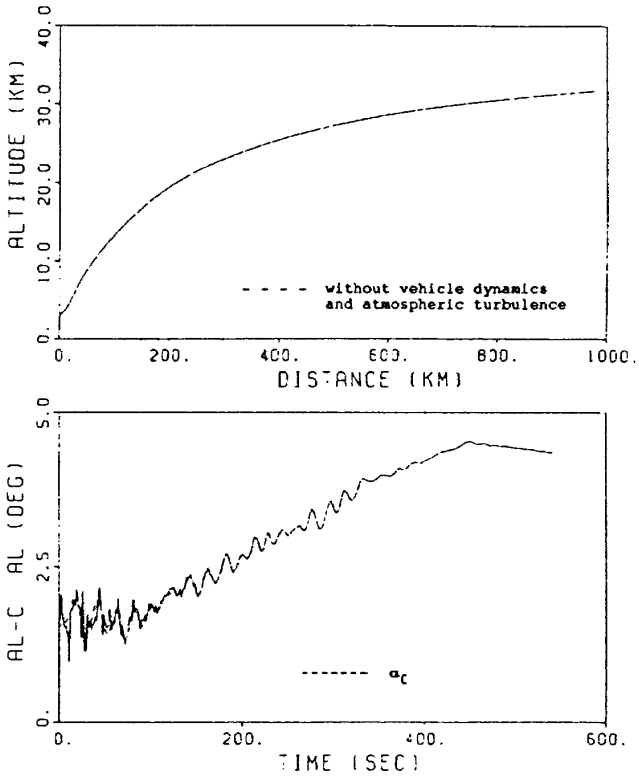

(c) Commanded angle of attack α_c and angle of attack α: altitude vs. distance

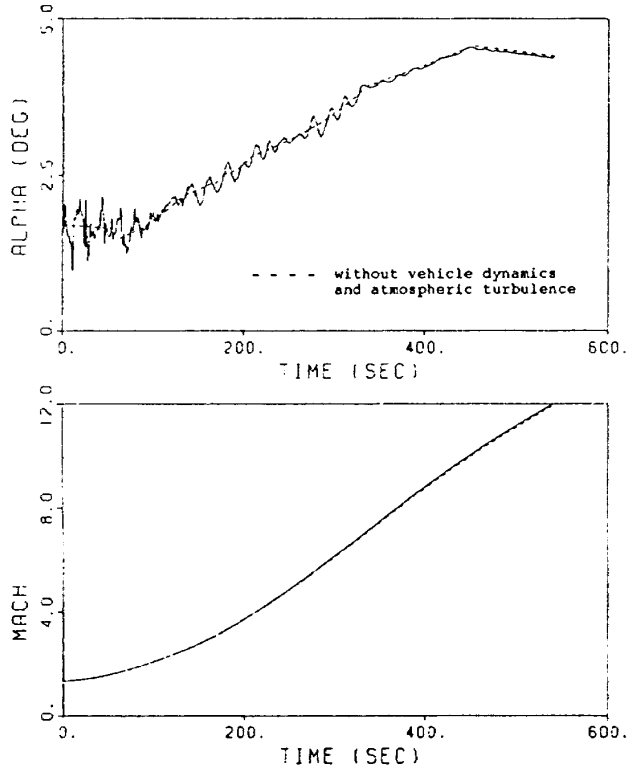

(b) Mach Number, angle of attack

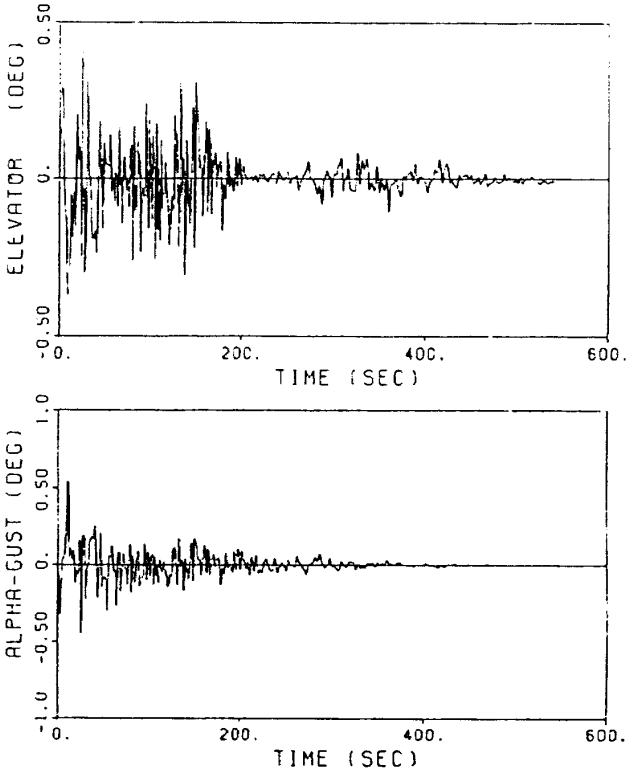

(d) Additional angle of attack due to atmospheric turbulence, elevator deflection

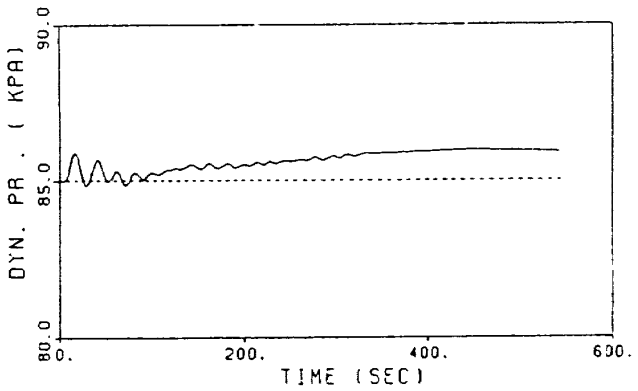

(e) Dynamic pressure

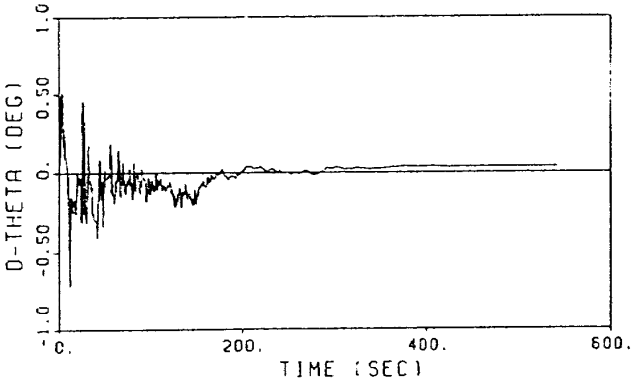

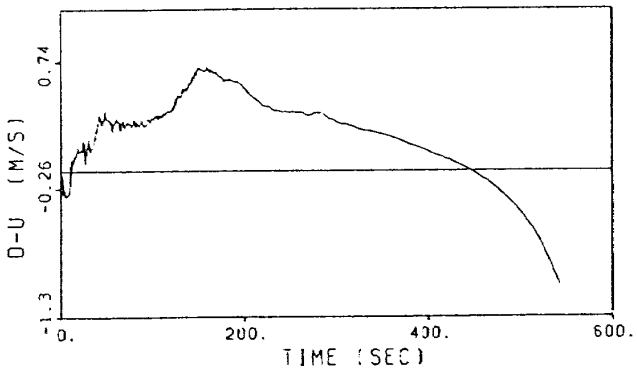

(f) Small disturbance state variables: Δu, $\Delta \theta$

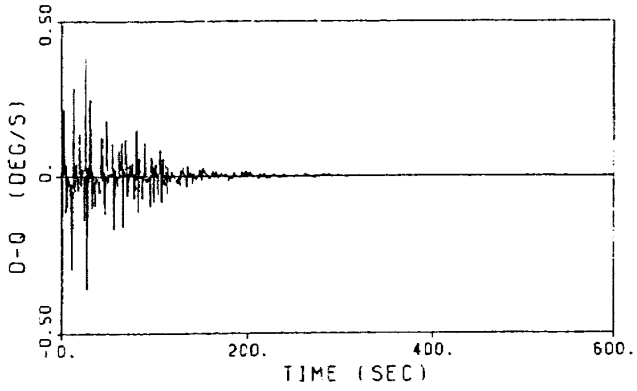

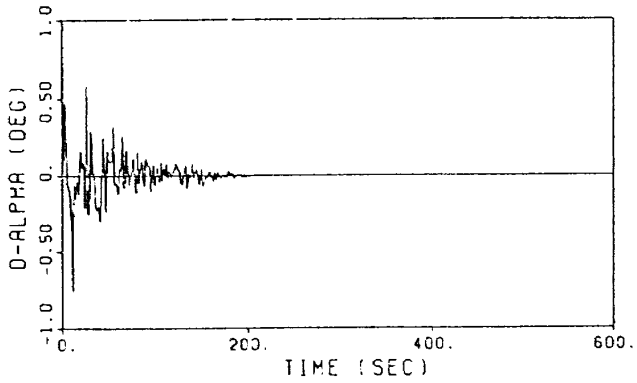

(g) Small disturbance state variables: $\Delta \alpha$, Δq

7. CONCLUSION

Flight mechanical derivatives and system data of NAL Spaceplane have been collected at seven reference Mach numbers (1.5, 2, 3, 4, 7.1, 10, 12) on a constant dynamic pressure ascent trajectory and a stability analysis of rigid Spaceplane was conducted.

For the Mach number step-size considered, small perturbation stability analysis shows that the short period motion is unstable and non-periodic at high Mach numbers beginning at M=4. For the dutch-roll motion instability begins at Mach number 7.1. The spiral motion is unstable for the Mach numbers 7.1, 10 and 12. The roll motion and phugoid motion remain stable throughout the considered trajectory.

Consequently a linear output feedback control law was introduced to achieve stable flight with favorable flight dynamic characteristics through-

out the whole ascent trajectory as recommended by commonly used handling quality criteria.

The decrease of natural stability and control effectiveness with increasing Mach number results in large feedback gain constants at high Mach numbers. Except for the yaw-axis control, a remarkable alleviation of feedback gain constants can be achieved if only 'acceptable' instead of 'desired' handling qualities are aspired during the feedback control design. The gain constants for the yaw-axis control remain high because of the very low rudder-effectiveness at high Mach numbers and the condition that the Dynamic Directional Stability Parameter has to exceed a limit value to ensure effectiveness of ordinary lateral/directional flight control methods. The permission of only 'acceptable' handling qualities by demanding minimum feedback gain constants is however accompanied by a higher sensitivity of the pole locations to changes in the gain constants. Hence, this controller design has a lower robustness.

Simulation of Spaceplane's ascent in the longitudinal plane for the presence of standard clear air turbulence and for a feedback control law achieving 'desired' flight dynamic behaviour shows, that the elevator deflection angles necessary to stabilize Spaceplane and to control the disturbances caused by the turbulence remain tolerable.

Future work has to deal with a complete six degree of freedom simulation of Spaceplane ascent in disturbed atmosphere. Possibly, measures to increase control effectiveness for the yaw-axis control at high Mach numbers might appear to be necessary.

Future work also has to answer the question to what extent handling quality criteria for conventional aircraft are applicable to a new generation super- and hypersonic transport vehicle like Spaceplane.

8. ACKNOWLEDGEMENT

One of the authors, Andreas Diekmann stayed at National Aerospace Laboratory as visiting researcher, from February 1989 to May 1990, sponsored by the European Communities Scientific Training Program in Japan and would like to thank the Laboratory for its kind hospitality. The authors wish to thank to many members of Aerodynamics Division and Control Systems Division for their assistance and valuable discussions during this study, and also to Miss S. Sekimori for her detailed typing and proofreading.

9. REFERENCES

1) Shirouzu, M, ; Matsushima, K. ; Nomura, S. : *A Parametric Study on the Ascent of a SSTO ;* Proc. 16th. Intern. Sympos. on Space Tech. and Sci. (ISTS), Sapporo 1988.

2) Nomura, S. ; Hozumi, K. ; Kawamoto, I. ; Miyamoto, Y. : *Experimental Studies on Aerodynamic Characteristics of SSTO Vehicle at Subsonic to Hypersonic Speeds ;* Proc. 16th. Intern. Sympos. on Space Tech. and Sci. (ISTS), Sapporo 1988.

3) unpublished data received from National Aerospace Laboratory, Tokyo, 1989.

4) Yamanaka T. : *The Japanese Spaceplanes R & D Overview ;* AIAA Second International Aerospace Planes Conference, Orlando, AIAA-90-5202, Oct. 1990.

5) Sakata, K. ; Matsumoto, N. ; Ohkami, Y. ; Matsushima, K. ; Yanagi, R. ; Shindo, S. : *System Study on Airbreathing Engine for Space Planes ;* Proc. of Aeroengine Conf. 1988, (in Japanese).

6) Masuya, G. ; Wakamatsu, Y. : *Calculation of SCRAM Jet Performance ; NAL* TM 598,

1988 (in Japanse)

7) Fehlberg, E. : *Classical Fifth-, Sixth-, Seventh- and Eighth- Order Runge Kutta Formulas With Stepsize Control* ; NASA TR R-287, Oct. 1968

8) Ashley H. ; Zartarian G. : *Piston theory-a new aerodynamic tool for the aeroelastician* ; J. of the Aeronautical Sciences, Vol. 23, Dec. 1956

9) Miles, J. W. : *The potential theory of unsteady supersonic flow* ; Cambridge Univ. Press, England, 1959

10) Inatani, Y. : *High Speed and High Angle of Attack Wind Tunnel Test Results of the Winged Space Vehicle C-2* ; ISAS Rep. 623, Tokyo, Oct. 1987

11) Inatani, Y. : *High Speed and High Angle of Attack Aerodynamic Characteristics of Winged Space Vehicle ; ISAS Rep. 624, Tokyo, Dec. 1987*

12) Etkin, B. : *Dynamics of Atmospheric Flight* ; John Wiley & Sons Inc., 1972

13) Wawrzyniak, M. E. : *To What Extent Should Space Shuttle Stability and Control be Provided Trough Stability Augmentation ? ; NASA TMX 52876, 1970*

14) Gamble, J. D. ; Spratlin, K. M. ; Skalecki, L. M. : *Lateral Directional Requirements for a Low L/D Aeromaneuvering Orbital Transfer Vehicle* ; AIAA-84-2123, 1984

15) Innocenti, M. ; Thukral, A. : *Roll response criteria for high maneuverable aircraft using Gibson's Method* ; AIAA-89-3391-CP, 1989

16) FACOM FORTRAN SSL II program library, ed. 1981

17) Nelson, R. B. : *Simplified Calculation of EigenvectorDerivatives* ; AIAA Journal Vol. 14, No. 9, September 1976

18) Weissmann R. : *Status of design criteria for predecting departure characteristics and spin susceptibility* ; J. Aircraft, Vol. 12, Dec. 1975

19) Inatani, Y. ; Yonemoto, K. : *Aerodynamic Design of Winged Space Vehicle* ; Proc. 16th. Intern. Sympos. on Space Tech. and Sci. (ISTS), Spporo 1988, pp. 1555-1562

20) Jacob, H. G. : *An Engineering Optimization Method with Application to STOL- Aircraft Approach and Landing Trajectories* ; NASA TN D-6978, 1972

21) Etkin, B. : *Turbulent Wind and Its Effect on Flight* ; Journal Aircraft, Vol. 18, No. 5, May 1981

22) Justus, C. G. : *New Height-Dependent Magnitudes And Scales For Turbulence Modeling* ; AIAA-89-0788, 1989

23) Schneider C. P. : *Analytic determination of dynamic stability parameters* ; AGARD-LS-114, rep. no.12, may 1981

24) Brune G. W. ; Dusto A. R. : *Slowly oscillating lifting surfaces at subsonic and supersonic speeds* ; J. Aircraft, Vol. 9, No. 11, Nov. 1972

25) Yanagizawa, M. ; Watanabe, S. : *Aerodynamic Coefficients of NAL Spaceplane from Newtonian Inpact Theory* ; unpublished data of National Aerospace Laboratory, Tokyo, 1989

26) Yonemoto, K. ; Mugitani, T. ; Makino, T. : *Stability Analysis Of Atmospheric Trajectory Of Space Plans For Dynamic Pressure/Heat-Input Rate Control* ; DGLR (Deutsche Gesellschaft für Luft-und Raumfahrt) annual meeting, Hamburg, 2.-4. oct. 1989

APPENDIX

Appendix 1 : Characteristic data at the considered seven reference points

1. Definition of aerodynamic coefficients and derivatives

a) aerodynamic coefficients

$C_X = X/Q\ S$ $\qquad$ $C_l = L/Q\ Sb$

$C_Y = Y/Q\ S$ $\quad C_m = M/Q\ Sc$

$C_Z = Z/Q\ S$ $\quad C_n = N/Q\ Sb$

b) aerodynamic derivatives

$C_{X\alpha} = \partial C_X/\partial\alpha$ $\quad C_{Xq} = \partial C_X/\partial\,(qc/2V_0)$

$C_{Y\beta} = \partial C_Y/\partial\beta$ $\quad C_{Yp} = \partial C_Y/\partial\,(pb/2V_0)$

$C_{Yr} = \partial C_Y/\partial\,(rb/2V_0)$ $\quad C_{Y\delta a} = \partial C_Y/\partial\delta_a$

$C_{Y\delta r} = \partial C_Y/\partial\delta_r$

$C_{Z\alpha} = \partial C_Z/\partial\alpha$ $\quad C_{Z\dot{\alpha}} = \partial C_Z/\partial\,(\dot{\alpha}c/2V_0)$

$C_{Zq} = \partial C_Z/\partial\,(qc/2V_0)$ $\quad C_{Z\delta e} = \partial C_Z/\partial\delta_e$

$C_{l\beta} = \partial C_l/\partial\beta$ $\quad C_{lp} = \partial C_l/\partial\,(pb/2V_0)$

$C_{lr} = \partial C_l/\partial\,(rb/2V_0)$ $\quad C_{l\delta a} = \partial C_l/\partial\delta_a$

$C_{l\delta r} = \partial C_l/\partial\delta_r$

$C_{m\alpha} = \partial C_m/\partial\alpha$ $\quad C_{m\dot{\alpha}} = \partial C_m/\partial\,(\dot{\alpha}c/2V_0)$

$C_{mq} = \partial C_m/\partial\,(qc/2V_0)$ $\quad C_{m\delta e} = \partial C_m/\partial\delta_e$

$C_{n\beta} = \partial C_n/\partial\beta$ $\quad C_{np} = \partial C_n/\partial\,(pb/2V_0)$

$C_{nr} = \partial C_n/\partial\,(rb/2V_0)$ $\quad C_{n\delta a} = \partial C_n/\partial\delta_a$

$C_{n\delta r} = \partial C_n/\partial\delta_r$

where :

S = wing reference area

c = mean aerodynamic chord

b = wing span

Vo = flight velocity at reference point

2. Reference conditions and aerodynamic derivatives Reference conditions at the seven points are shown in Table A. 1 and also aerodynamic derivatives in Table A. 2 and A. 3.

Table A. 1 Reference conditions and aerodynamic derivatives

Reference conditions:

(Time = 0 s for Mach = 1.33)

Mach	1.5	2	3	4	7.1	10	12
Time (s)	41	93	164	214	338	453	546
m (to)	327.5	320.9	312.6	307.6	292.6	276.6	262.7
I_{xx} (Nm^2)	$5.45\cdot10^6$	$5.33\cdot10^6$	$5.17\cdot10^6$	$5.07\cdot10^6$	$4.84\cdot10^6$	$4.63\cdot10^6$	$4.47\cdot10^6$
I_{yy} (Nm^2)	$35.90\cdot10^6$	$35.10\cdot10^6$	$34.00\cdot10^6$	$33.30\cdot10^6$	$31.70\cdot10^6$	$30.30\cdot10^6$	$29.10\cdot10^6$
I_{zz} (Nm^2)	$40.10\cdot10^6$	$39.10\cdot10^6$	$37.90\cdot10^6$	$37.10\cdot10^6$	$35.40\cdot10^6$	$33.80\cdot10^6$	$32.50\cdot10^6$
α_0 (deg)	1.667	1.69	2.37	2.85	3.933	4.56	4.40
γ_0 (deg)	7.33	6.16	4.23	3.10	1.233	0.572	0.333
v_0 (m/s)	527.1	700.8	1012	1310	2190	2971	3493
h_0 (m)	4935	8978	14190	17840	25130	29480	31740
T_0 (kN)	3110	3240	3150	3190	3170	2770	2320
$C_{L,0}$	0.0726	0.0622	0.0614	0.0577	0.0516	0.0455	0.0412
$C_{D,0}$	0.0416	0.0376	0.0277	0.0224	0.0214	0.0224	0.0218

Trim conditions (for Mach Numbers with windtunnel data available):
(center of gravity at 68% length from nose)

with canards (δ_c = 2 deg):

Mach	1.5	2	3	4
$C_{m,0}$	0.0198	0.0127	0.00624	0.00506
$\delta_{e,trim}$ (deg)	6.4	6.0	4.7	4.8

without canards:

Mach	1.5	2	3	4	7.1
$C_{m,0}$	-0.00228	-0.00638	-0.00768	-0.00753	-0.0041
$\delta_{e,trim}$ (deg)	-0.7	-3.0	-5.7	-7.2	-10.6

Table A. 2 Aerodynamic derivatives of the spaceplane without canards

Mach	1.5	2	3	4	7.1	10	12
$C_{X\alpha}$	-0.01	-0.004	0.005	0.011	0.030	0.040	0.048
C_{Xq}	-0.044	-0.0399	-0.0288	-0.0236	-0.007	0.0029	0.0014
$C_{Y\beta}$	-0.613	-0.517	-0.413	-0.355	-0.329	-0.329	-0.329
C_{Yp}	-0.074	-0.062	-0.050	-0.045	-0.040	-0.038	-0.036
C_{Yr}	-0.196	-0.194	-0.190	-0.201	-0.212	-0.212	-0.231
$C_{Y\delta a}$	0	0	0	0	0	0	0
$C_{Y\delta r}$	0.069	0.061	0.042	0.025	0	0	0
$C_{Z\alpha}$	-2.42	-2.04	-1.53	-1.24	-0.690	-0.565	-0.507
$C_{Z\dot{\alpha}}$	-0.115	-0.103	-0.0589	-0.0230	-0.0038	-0.0014	-0.00078
C_{Zq}	-0.0373	0.0546	0.1717	0.2558	0.3819	0.4213	0.4639
$C_{Z\delta e}$	-0.222	-0.141	-0.093	-0.065	-0.0184	-0.017	-0.016
$C_{l\beta}$	-0.0726	-0.0605	-0.030	-0.0161	-0.0081	-0.007	-0.0060
C_{lp}	-0.1933	-0.160	-0.117	-0.0967	-0.0616	-0.0466	-0.0419
C_{lr}	0.0652	0.0543	0.0407	0.0345	0.0224	0.0167	0.0153
$C_{l\delta a}$	0.069	0.051	0.039	0.027	0.009	0.004	0.0035
$C_{l\delta r}$	0.0145	0.0110	0.0073	0.0054	0.0023	0.0012	0.0010
$C_{m\alpha}$	-0.702	-0.437	-0.167	0.0131	0.0729	0.085	0.090
$C_{m\dot{\alpha}}$	0.0054	-0.0036	-0.0078	-0.0060	-0.00145	-0.00062	-0.0001
C_{mq}	-4.367	-3.709	-2.899	-2.564	-1.953	-1.679	-1.636
$C_{m\delta e}$	-0.1775	-0.121	-0.0767	-0.060	-0.0222	-0.02	-0.019
$C_{n\beta}$	0.258	0.178	0.076	0.025	-0.0176	-0.030	-0.035
C_{np}	0.0652	0.0543	0.0407	0.0345	0.0224	0.0167	0.0153
C_{nr}	-0.713	-0.620	-0.501	-0.457	-0.368	-0.324	-0.332
$C_{n\delta a}$	0	0	0	0	0	0	0
$C_{n\delta r}$	-0.038	-0.030	-0.0185	-0.013	-0.0050	-0.0027	-0.0024

Table A. 3 Aerodynamic derivatives of the spaceplane with canards

Mach	1.5	2	3	4
$C_{X\alpha}$	-0.0124	-0.0134	0.0013	0.0062
C_{Xq}	-0.0446	-0.0399	-0.0288	-0.0237
$C_{Y\beta}$	-0.613	-0.517	-0.413	-0.355
C_{Yp}	-0.074	-0.062	-0.050	-0.045
C_{Yr}	-0.196	-0.194	-0.190	-0.201
$C_{Y\delta a}$	0	0	0	0
$C_{Y\delta r}$	0.069	0.061	0.042	0.025
$C_{Z\alpha}$	-2.41	-2.08	-1.43	-1.28
$C_{Z\dot{\alpha}}$	-0.115	-0.103	-0.0589	-0.0230
C_{Zq}	0.2014	0.2507	0.3147	0.3736
$C_{Z\delta e}$	-0.222	-0.141	-0.093	-0.065
$C_{l\beta}$	-0.0726	-0.0605	-0.030	-0.0161
C_{lp}	-0.1969	-0.1620	-0.119	-0.0984
C_{lr}	0.0652	0.0543	0.0407	0.0345
$C_{l\delta a}$	0.069	0.051	0.039	0.027
$C_{l\delta r}$	0.0145	0.0110	0.0073	0.0054
$C_{m\alpha}$	-0.235	-0.151	-0.0566	0.0141
$C_{m\dot{\alpha}}$	-0.0172	-0.0180	-0.0124	-0.0089
C_{mq}	-4.806	-4.070	-3.165	-2.783
$C_{m\delta e}$	-0.1775	-0.121	-0.0767	-0.060
$C_{n\beta}$	0.258	0.178	0.076	0.025
C_{np}	0.0652	0.0543	0.0407	0.0345
C_{nr}	-0.713	-0.620	-0.501	-0.457
$C_{n\delta a}$	0	0	0	0
$C_{n\delta r}$	-0.038	-0.030	-0.0185	-0.013

Appendex 2 Computation of rotary aerodynamic derivatives in the super- and hypersonic flight regime with Piston theory

To obtain an estimation of the rotary stability derivatives of Spaceplane in the investigated super-and hypersonic flight regime for the purpose of flight dynamic analysis, Piston theory was employed as an easy-to- use method.

A FORTRAN program was generated to calculate the rotary stability derivatives of Spaceplane with and without canards and for the Mach numbers and angles of attack occurring during the analysed ascent trajectory.

1. Description of the method

Piston theory assumes that the local pressure on an surface is related to the local normal component of the surface's velocity relative to the fluid like the pressure on the face of a piston moving in a one-demensional channel is related to the velocity of its motion.

The relative velocity of the surface relative to the fluid may be due to the inclination of the surface to the direction of the fluid flow or due to a motion of the surface itself.

According to Ashley, ref. 8, "in general, Piston theory may be employed for large flight Mach numbers or high reduced frequencies of unsteady motion, whenever the surface involved is nearly plane and not inclined too sharply to the direction of the free stream". Because of the low angle of attack during the considered ascent trajectory and because of Spaceplane's body shape the restriction for the surface inclination is fulfilled with the exception of small areas near the tip of the fuselage.

Under the assumption that only simple waves are generated and no entropy changes are produced, the exact expression for the pressure on the face of a piston moving with velocity w in a channel containing perfect gas is according to ref. 8 :

$$\frac{p}{p_\infty} = \left\{ 1 + {}^1/_2 \, (\tau - 1) \, \left(\frac{w}{a_\infty}\right) \right\}^{2\tau/(\tau-1)} \qquad (A2-1)$$

τ — ratio of specific heats (air : $\tau = 1.4$)

a_∞ — free stream speed-of-sound

P_∞ — free stream static pressure

From eqn. (A2−1) and with

$$p_\infty = \frac{\rho_\infty \, a_\infty{}^2}{\tau} \quad \text{and} \quad M = \frac{w_\infty}{a_\infty}$$

(w_∞ and P_∞ are the velocity and airdensity of the free stream) the pressure coefficient C_p can be written as :

$$c_p = \frac{p - p_\infty}{1/2 \, \rho_\infty \, w_\infty{}^2}$$

$$= \frac{2}{\tau M^2} \left\{ \left[1 + \frac{\tau - 1}{2} \frac{w}{a_\infty} \right]^{(2\tau/\tau-1)} - 1 \right\} \qquad (A2-2)$$

A surface element (fig. A−1) is defined by a surface area A, the unit normal vector $\{n\}$ and a vector of length R and direction $\{\gamma\}$ between the origin of the reference coordinate system and the surface reference point. This surface element is located in an airflow, defined

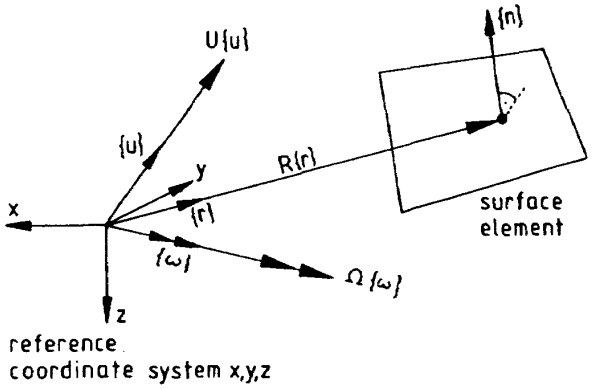

Fig. A−1. Definition of a surface element

by the velocity U and the direction $\{u\}$, and rotates around an axis defined by the direction $\{w\}$ with an angular velocity Ω. $\{r\}$, $\{u\}$ and $\{w\}$ are all unit vectors.

The velocity w normal to the surface consists of a static portion w_{stat} which is proportional to the inclination of the surface to the direction of the undisturbed airflow, and of a dynamic portion w_{dyn} proportional to the relative velocity induced by the rotation.

$$w = w_{stat} + w_{dyn} \qquad (A2-3)$$

The static portion w_{stat} can be written as :

$$w_{stat} = U\{u\}^T\{n\} \equiv U\ s_1 \qquad (A2-4)$$

where :

$$\{u\} = \begin{Bmatrix} \cos\beta & \cos\alpha \\ \sin\beta & \\ \mathrm{coa}\,\beta & \sin\alpha \end{Bmatrix} \qquad (A2-5)$$

α and β are the angles of attack and sideslip of the body to which the surface element belongs.

The dynamic portion w_{dyn} can be written as :

$$w_{dyn} = \Omega R\left(\{\omega\} \times \{r\}\right)^T\{n\} \equiv \Omega R\, s_2 \qquad (A2-6)$$

('x' indicates the vector product)

Introducing a normalized angular velocity Ω^* :

$$\Omega^* = \frac{\Omega}{U/1_{ref}} \qquad (A2-7)$$

where l_{ref} is a reference length. The rotary derivative $C_{p\Omega}$ defined at $\Omega^* =$ is :

$$C_{p\Omega} = \frac{\partial C_p}{\partial \Omega^*} \equiv \frac{\partial C_p}{\partial w_{dyn}} \frac{\partial w_{dyn}}{\partial \Omega^*} \Bigg|_{\Omega^*=0} \qquad (A2-8)$$

with eqn. (A2−6) and (A2−2) follows :

$$C_{p\Omega} = 2\frac{R}{M1_{ref}} s_2 \left[1 + 1/2\,(\tau-1)\,M s_1\right]^{(\tau+1)/(\tau-1)} \qquad (A2-9)$$

After multiplying eqn. (A2−9) with the surface normal vector $\{n\}$, the rotary derivatives of the aerodynamic forces in the bodyfixed coordinate system can be obtained

$$\begin{Bmatrix} C_{X\Omega} \\ C_{Y\Omega} \\ C_{Z\Omega} \end{Bmatrix}' = C_{p\Omega}\{n\} \qquad (A2-10)$$

The derivatives of the aerodynamic moments are :

$$\begin{Bmatrix} C_{l\Omega} \\ C_{m\Omega} \\ C_{n\Omega} \end{Bmatrix}' = C_{p\Omega}\{n\} \times \left(R\{r\} - R_0\{r\}_0\right) \qquad (A2-11)$$

where $R_0\{r\}_0$ defines the moment reference point in the bodyfixed coordinate system.

The mark $'$ indicates, that the derivatives are with respect to one surface panel.

If consequently $\{\omega\}$ in eqn. (A2−6) is chosen to be aligned with the bodyfixed axis, i. e. the rotations are either pure rolling, pitching or yawing motions, the rotary derivatives C_{Xp}, C_{Xq}, C_{Xr}, $C_{Yp}, \cdots$, C_{nr} can be obtained.

The sum of the rotary derivatives for all surface panels weighted with the respective surface area A_i leads to the rotary derivatives of the whole body :

$$C_{ab} = 1/A_{ref} \sum_{i=1}^{k} C_{ab,i}' A_i \qquad (A2-12)$$

where k is the number of surface panels. The index 'a' stands for one index out of X, Y,

Z, l, m, n and 'b' for one index out of p, q, r. A_{ref} is the vehicle reference area.

According to ref. 23 Piston theory results can be improved by replacing the constant factor (named C subsequently) of 2 in eqn. (A2-9) by the normal force slope $C_{N\alpha}$. In this paper the constant value of C=2 is replaced by a factor F which is computed as

$$F = \frac{N_{\text{measured}}(\alpha)}{N_{\text{piston}}(C=1,\ \alpha)} \qquad \text{(A2-13)}$$

$N_{Piston}(C=1,\ \alpha)$ is the aerodynamic normal force as computed by Piston-theory assuming a constant factor of C=1 instead of C=2. $N_{measured}(\alpha)$ is the value of the normal force as measured in the windtunnel. This means, the factor F is chosen in a way, that the normal force measured and the normal force calculated by Piston-theory employing the factor F instead of 2 in eqn.(A2-9) – assume the same value.

To avoid the large relative error in the windtunnel results in the region of small normal forces (i.e. at small angles of attack) F is computed only once for each Mach number, namely for the angle of attack of 5 deg.

The FORTRAN program installed allows the treatment of aircraftbodies which surface is defined by quadrangular panels[7] defined by the coordinates of the four corner-points ($\{r\}_i$, i=1, 2,3,4) in the bodyfixed coordinate system. The panel reference point is defined by the mean value of the coordinates of these four corner points (see fig. A-2):

$$\{r\} = 1/4\left(\{r\}_1 + \{r\}_2 + \{r\}_3 + \{r\}_4\right) \qquad \text{(A2-14)}$$

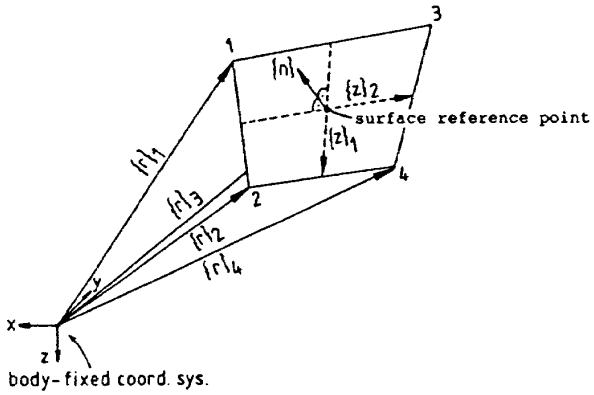

Fig. A-2 Definition of a quadrangular panel

The vector {n} normal to the panel and of unit length is defined as :

$$\{n\} = \left(\{z\}_1 \times \{z\}_2\right) / \left|\{z\}_1 \times \{z\}_2\right| \qquad \text{(A2-15)}$$

where the operator 'x' denotes a vector product and '|.|' denotes the amount of a vector. The vectors {z} 1 and {z} 2 are :

$$\{z\}_1 = \{r\}_2 - \{r\}_1 + \{r\}_4 - \{r\}_3 \qquad \text{(A2-16)}$$

$$\{z\}_2 = \{r\}_3 - \{r\}_1 + \{r\}_4 - \{r\}_2 \qquad \text{(A2-17)}$$

2. Application of Piston Theory to a delta wing

To obtain a feeling for the quality of Piston theory results, fig. A-3 compares the damping derivatives C_{Lq} and C_{Mq} of a delta wing computed by Piston theory (F=2) and by two other methods (ref.9, 24) which are more laborious

7) In the practical application of Piston theory to a panel element it has to be distinguished whether the panel is wetted by the airflow from only one or from both sides. For example panels belonging to the fuselage are usually wetted only from one side.

than Piston theory and also more suitable for lower Mach numbers.

Fig. A-3 shows, that even for a Mach number as low as 1. 4, the difference between these results is small enough to take Piston theory as an easy-to-use method for the calculation of rotary derivatives for an application on flight dynamic analysis.

3. Application of Piston theory to Spaceplane

Piston theory will now be applied to compute the rotary derivatives of Spaceplane for M=1.5 to 12.

The body shape of Spaceplane is represented by the grid of quadrangular surface panels as shown in fig.A-4.

The grid employed for this calculation of 918 panels (fuselage : 270 panels, right and left wing each : 300 panels ; vertical tails each : 16 panels ; winglets each : 8 panels (panels of vertical tails and winglets are wetted from both sides))

Because of the symmetric flight conditions investigated ($\beta=0$), the symmetry of Spaceplane with respect to the x/z-plane and because of the properties of Piston theory, rolling and yawing motion only induce lateral forces and moments while pitching motion only generates longitudinal forces and moments. Fig. A-5 shows Piston theory results for the rotary stability derivatives of Spaceplane for an angle of attack $\alpha=0°$. For comparison results obtained with Newtonian Impact Theory (ref. 25) are shown with a dashed line. Newtonian Impact Theory gives good results at very high Mach numbers.

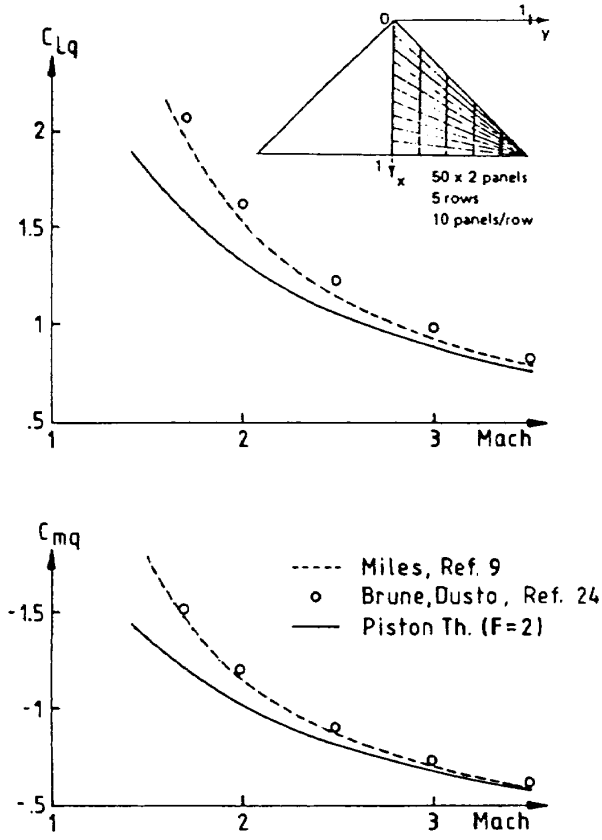

Fig. A-3. Comparison of Piston Theory results with different computational methods

Appendix 3 Stability analysis of constant dynamic pressure trajectory control[8]

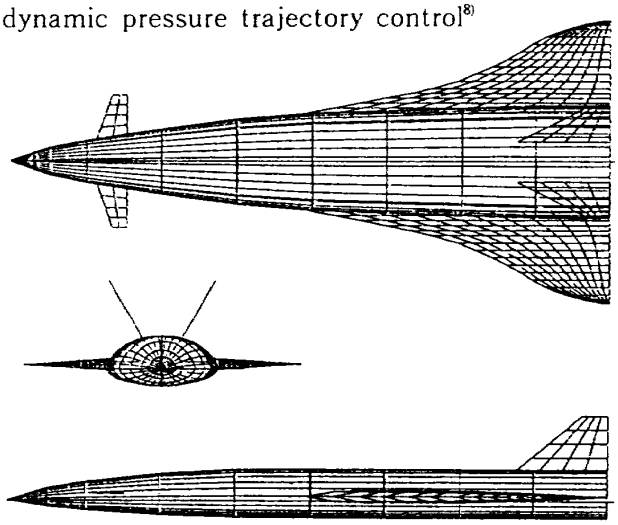

Fig. A-4. Surface grid for computation of Spaceplane rotary derivatives with Piston Theory

8) A detailed discussion on the stability of a constant dynamic pressure/heat input rate trajectory is given in ref. 26.

The dynamic pressure is controlled by a simple linear feedback of the deviation of the dynamic pressure from the nomial value to generate a commanded angle of attack input :

$$\alpha_C = K\,(Q - Q_0),\quad Q_0 = 85\,\text{kpa} \qquad \text{(A3-1)}$$

Regarding Spaceplane as a mass point the equations of motion for the flight velocity, flight path angle and dynamic pressure (see. eqn.(1), (2) and (3)) were linearized and written in vector form :

$$\{\dot{x}\} = [A]\{x\} + \{b\}\alpha_C \qquad \text{(A3-2)}$$

$$\{\dot{x}\} = [A]\{x\} + \{b\}\{s\}^T\{x\} \qquad \text{(A3-3)}$$

$$\{x\}^T = \{\, \Delta V,\ \Delta\nu,\ \Delta Q \,\} \qquad \text{(A3-4)}$$

$$\{s\}^T = \{\, 0,\ 0,\ K \,\} \qquad \text{(A3-5)}$$

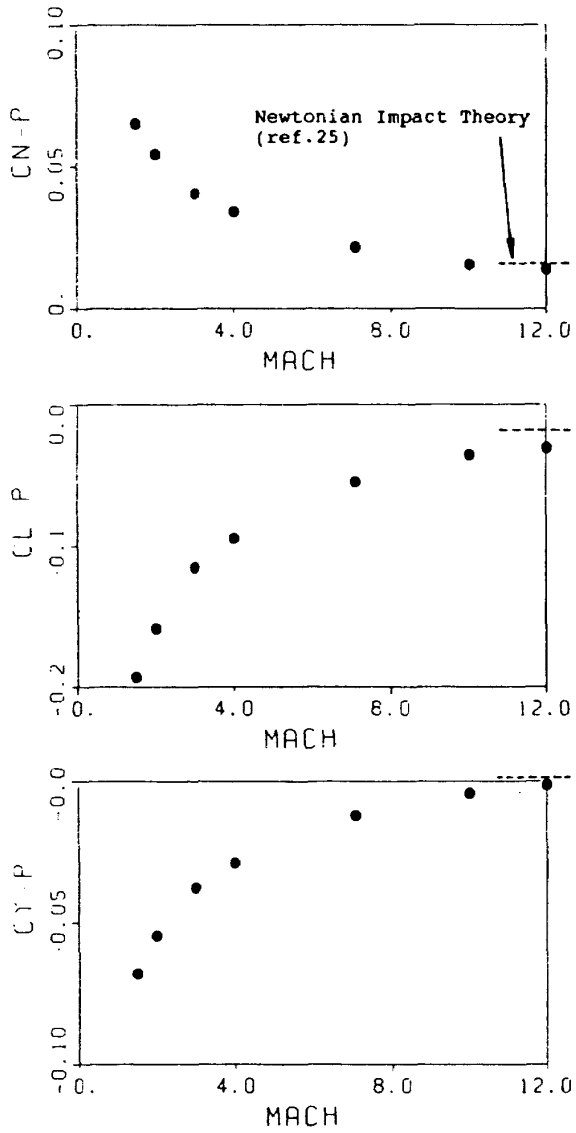

Fig. A-5. Rotary derivatives of Spaceplane vs. Mach Number ($\alpha = 0$ deg., Piston Theory results)
(a) C_{Yp}, C_{lp}, C_{np}

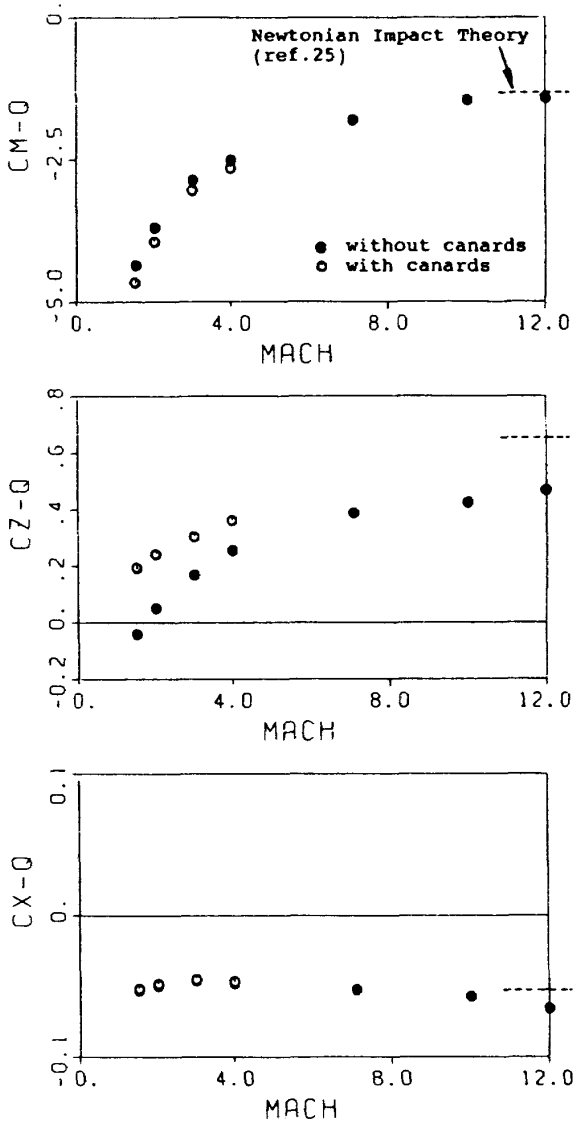

(b) C_{Xq}, C_{Zq}, C_{mq}

The matrix [A] and the vector {b} are :

$$[A] = \qquad \text{(A3-6)}$$

$$\left[\begin{array}{c|c|c} -\frac{\rho V}{m}SC_D & -g\cos\nu & -\frac{SC_D}{m} \\ -\frac{T}{mV^2}\sin\alpha+\left(\frac{g}{V^2}+\frac{1}{R}\right)\cos\nu+\frac{S\rho C_L}{2m} & \left(\frac{g}{V}-\frac{V}{R}\right)\sin\nu & \frac{SC_L}{mV} \\ -2\frac{Q}{h_s}-\sin\nu-(\rho V)^2\frac{SC_D}{m} & -\left(\frac{Q}{h_s}+\rho g\right)V\cos\nu & -\rho V\frac{SC_D}{m} \end{array}\right]$$

$$\{b\}=\left\{\begin{array}{l} -\frac{T}{m}\sin\alpha-\frac{Q}{m}SC_{D\alpha} \\ \frac{T}{mV}\cos\alpha+\frac{Q}{mV}SC_{L\alpha} \\ \rho V\left(-\frac{T}{m}\sin\alpha-\frac{Q}{m}SC_{D\alpha}\right) \end{array}\right\} \qquad \text{(A3-7)}$$

The root loci of the closed loop system, that are the eigenvalues of the augmented system matrix [A]*

$$[A]^*=[A]+\{b\}\{s\}^T \qquad \text{(A3-8)}$$

were computed for the seven reference conditions. The conjugate complex eigenvalue represents a phugoid-type motion, the nonoscillatory

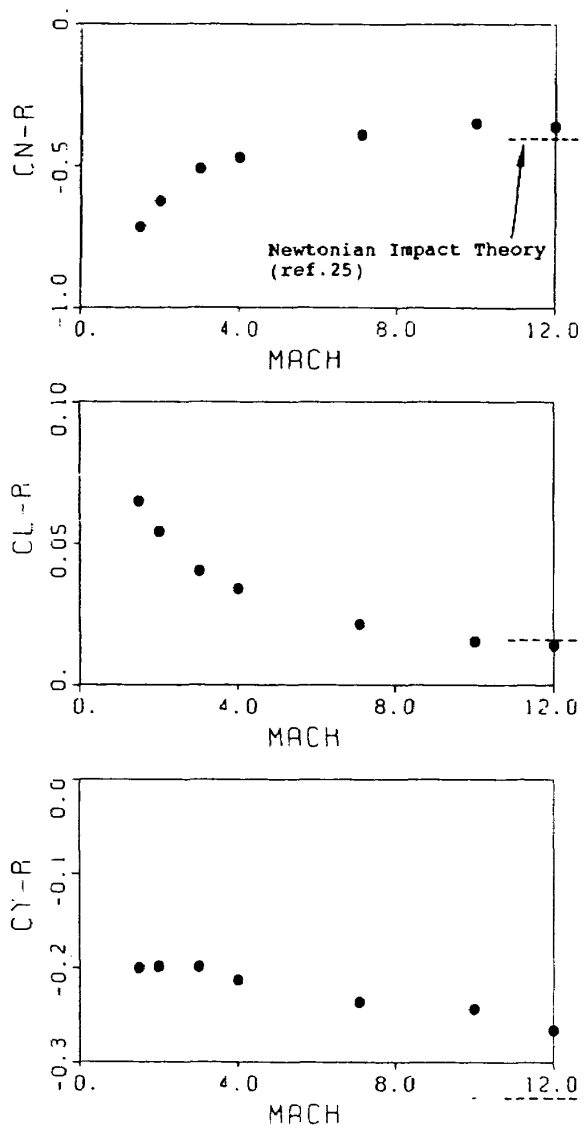

(c) C_{Y_β}, C_{l_β}, C_{n_β}

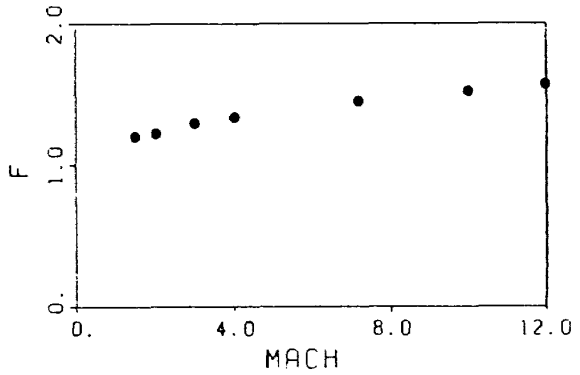

(d) Factor F (see eqn. A2-13)

eigenvalue describes a motion which only exists in case of an altitude dependent air density. In case of a constant air density, that means the characteristic length h_s would be infinity (see eqn. (5)), the first and third line in the system matrix [A]* would become linear dependent so only the phugoid-type solution would remain.

As an example for the computation, the root loci for the Mach number M=7.1 reference point are shown in fig. A-6 for different control parameters K. As can be seen from the location of the zeros of the open loop system, for sufficiently large feedback constants K, all closed loop poles can be shifted to have a negative real part.

The factor K=0.125 [deg/kpa] which is used for Spaceplane ascent trajectory control simulation at M=7.1 in chapter 6 has only a minor effect on the phugoid type motion but leads to a shift of the pole of the non-oscillatory mode towards negative real parts. Hence, by employing this feedback constant, the ascent is a stable motion at this Mach number.

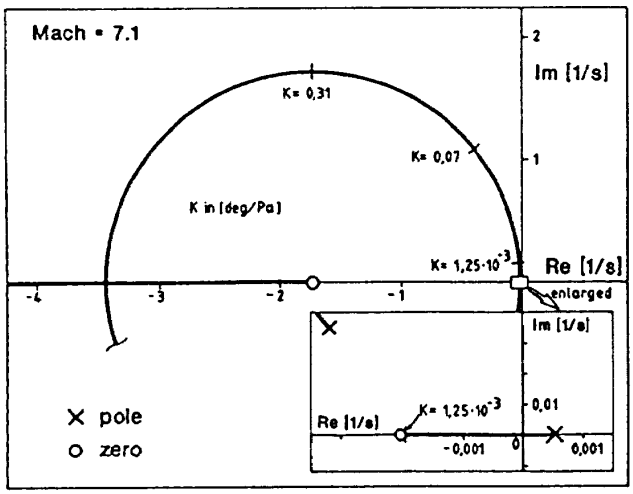

Fig. A−6 Ascent trajectory stability analysis (root loci for Mach Number 7.1)

TECHNICAL REPORT OF NATIONAL
AEROSPACE LABORATORY
TR-1128T

航空宇宙技術研究所報告1128T号(欧文)

平成3年11月発行

発行所 航空宇宙技術研究所
東京都調布市深大寺東町7丁目44番地1
電話三鷹(0422)47-5911(大代表)〒182
印刷所 株式会社 セイコー社
東京都調布市西つつじヶ丘1丁目5番地15

Published by
NATIONAL AEROSPACE LABORATORY
7-44-1 Jindaijihigashi-Machi Chofu, Tokyo
JAPAN

Printed in Japan